NASA CONTRACTOR REPORT

NASA CR-25
VOL

NASA CR-2559
VOL. I

NUMERICAL NONLINEAR INELASTIC ANALYSIS OF STIFFENED SHELLS OF REVOLUTION

Volume I - Theory Manual for STARS-2P Digital Computer Program

V. Svalbonas and H. Levine

Prepared by
GRUMMAN AEROSPACE CORPORATION
Bethpage, N.Y. 11714

for George C. Marshall Space Flight Center

NATIONAL AERONAUTICS AND SPACE ADMINISTRATION • WASHINGTON, D.C. • JULY 1975

TECHNICAL REPORT STANDARD TITLE PAGE

1. REPORT NO.	2. GOVERNMENT ACCESSION NO.	3. RECIPIENT'S CATALOG NO.
NASA CR-2559		

4. TITLE AND SUBTITLE	5. REPORT DATE
Numerical Nonlinear Inelastic Analysis of Stiffened Shells of Revolution, Volume I - Theory Manual for STARS-2P Digital Computer Program	JULY 1975
	6. PERFORMING ORGANIZATION CODE M142
7. AUTHOR(S) V. Svalbonas and H. Levine	8. PERFORMING ORGANIZATION REPORT #
9. PERFORMING ORGANIZATION NAME AND ADDRESS	10. WORK UNIT NO.
Grumman Aerospace Corp. Bethpage, NY 11714	11. CONTRACT OR GRANT NO. NAS8-28569
	13. TYPE OF REPORT & PERIOD COVERED Contractor Report
12. SPONSORING AGENCY NAME AND ADDRESS National Aeronautics and Space Administration Washington, D. C. 20546	14. SPONSORING AGENCY CODE

15. SUPPLEMENTARY NOTES

16. ABSTRACT

Volume I of this report contains the theoretical analysis background for the STARS-2P nonlinear inelastic program. The theory involved is amenable for the analysis of large deflection inelastic behavior in axisymmetric shells of revolution subjected to axisymmetric loadings. The analysis is capable of considering such effects as those involved in nonproportional and cyclic loading conditions.

This report is prepared in four volumes, The other volumes are:

Volume II — User's Manual for STARS-2P Digital Computer Program
Volume III — Engineer's Program Manual for STARS-2P Digital Computer Program
Volume IV — SATELLITE-1P Program for STARS-2P Digital Computer Program

17. KEY WORDS	18. DISTRIBUTION STATEMENT
	UNCLASSIED-UNLIMITED STAR CATEGORY 39

19. SECURITY CLASSIF. (of this report)	20. SECURITY CLASSIF. (of this page)	21. NO. OF PAGES	22. PRICE
Unclassified	Unclassified	52	$4.25

CONTENTS

FIGURES

SUMMARY

This report describes the latest addition to the STARS system of computer programs, STARS-2P, for the plastic, large deflection analysis of axisymmetrically loaded shells of revolution. The STARS system uses a numerical integration scheme to solve the governing differential equations. Several unique features for shell of revolution programs that are included in the STARS-2P program are described. These include orthotropic nonlinear kinematic hardening theory, a variety of shell wall cross sections and discrete ring stiffeners, cyclic and nonproportional mechanical and thermal loading capability, the coupled axisymmetric large deflection elasto-plastic torsion problem, an extensive restart option, arbitrary branching capability, and the provision for the inelastic treatment of smeared stiffeners, isogrid, and waffle wall constructions. To affirm the validity of the results, comparisons with available theoretical and experimental data are presented.

LIST OF SYMBOLS

Lower Case Latin:

e_{ij}	Linear strain
$\{f\}$	Local force matrix
h	Shell thickness
k	Shell curvature
$[k]$	Stiffness matrix
m	Distributed moment load
n	Fourier harmonic number
0	Subscript meaning reference surface
r_1	Meridional radius of curvature
r_2	Circumferential radius of curvature
r_c	Ring centroidal radius
r_0	Radius of revolution
s	Arc length
u	Circumferential shell displacement
v	Meridional shell displacement
w	Normal shell displacement (positive inward)

Upper Case Latin:

C	Eccentricity of reinforcement
D	Bending stiffness
E	Young's modulus
F	Distributed loads on the shell
G	Shear modulus
J	Effective transverse shear stress resultant
K	Extensional stiffness
M	Bending stress resultant
N	Membrane stress resultant
Q	Transverse shear stress resultant
T	Temperature
Z, R, θ	Global coordinate system

Greek

α	Coefficient of thermal expansion
ω	Rotation of the normal to the middle surface of the shell
ζ	Shell coordinate normal to the middle surface of the shell (positive inward)
θ, φ	Circumferential and meridional shell coordinates
σ_{ij}	Normal components of stress
ν	Poisson's ratio
τ_{ij}	Shearing components of stress
Δ	Deformation
$\{\delta\}$	Local displacement matrix

Other symbols are defined in the text where used.

INTRODUCTION TO NUMERICAL INELASTIC SHELL ANALYSIS

Recent innovations in digital computer technology allow designers to analyze shell structures of complex configurations without unduly restrictive approximations. A number of versatile computer programs, based on various methods of analysis, are presently available for the inelastic analysis of shells of revolution. These are briefly discussed, and categorized by the numerical method used, below.

Finite Element Method

Perhaps the earliest documented large deflection, shell analysis program available was MARC, Ref. [1]. This program has grown over the years to include elements not exclusively for shell of revolution analysis, and has become a general system for large deflection, inelastic analysis of structures, Ref. [2]. The program contains both isotropic and kinematic hardening theory, and is able to represent the material properties with linear hardening, and Ramberg-Osgood representations. The solution scheme utilizes the tangent modulus method and Gaussian elimination. The basic revolved elements used in this program are those due to Khojasteh-Bakht, Ref. [3]. A second program using these elements is due to Yaghmai, Ref. [4]. However, this was a small program (limited to 80 elements) containing isotropic hardening theory.

Another shell of revolution, finite element code (IBLAD) was developed by Zudans, Ref. [5]. The capability also included isotropic and kinematic hardening theories, with the solution process utilizing the tangent modulus method and Gaussian elimination. The experiences gained in formulating the above program were then utilized in creating a more general shell analysis program, EPACA, Ref. [6]. This program has the capability of elastic-plastic-creep analysis of thin or thick three-dimensional shells made up of curved or flat shell elements. Continuous or discrete elastic foundations are also included in the analysis. The program contains both isotropic and kinematic hardening theory, and is able to represent the material properties with linear hardening, and Ramberg-Osgood representations. The solution scheme utilizes the tangent modulus method and Gaussian elimination. Heat transfer analysis capability is in a developmental stage for this program, as is a completely new code, DYPLAS, Ref. [7], which will include dynamic effects.

Other finite element programs, tailored more exclusively to shells of revolution include those of Ref. [8, 9]. The DYNAPLAS program, Ref. [8, 10], is a small (limited to 50 elements and 20 Fourier harmonics) but sophisticated program which includes dynamic effects. It utilizes a modified Novozhilov, Ref. [11], shell theory, and contains both isotropic hardening and a mechanical sublayer model, Ref. [12]. The solution process utilizes the "right hand side" (initial strain or stress) technique, and a restart capability is available for longer problems. Rings and spring foundations can also be included

in the analysis. The AXSHEL program, Ref. [9], is actually a subprogram of the PLANS system, Ref. [13]. This system was designed and built specifically for nonlinear analysis (plasticity and large deflection) of structures, and includes, among others, special crack tip elements. The program uses kinematic hardening theory, and is able to represent the material properties with linear hardening, and Ramberg-Osgood representations. The solution schemes utilizes the right hand side technique and partitioning.

Other finite element, inelastic codes, which mainly do not use shell of revolution elements, but which nevertheless deserve mention, include ANSYS, Ref. [14], and NEPSAP, Ref. [15].

Finite Difference Method

Several special purpose finite difference inelastic analysis programs have been available for some time, Ref. [16-18]. The most general and recent of these, however, is PETROS2, Ref. [19, 20]. This program analyzes arbitrary thin shells using a two-dimensional finite difference space mesh, and expanding time also in central differences. First order difference formulas are used for all expansions. The mechanical sublayer model is used with integrations through the thickness being performed by Gaussian quadrature. Dynamic effects are considered.

A finite difference program recently being developed for inelastic shell of revolution analysis is BOSOR5, Ref. [21]. The numerical method used should actually be classified as variational finite-difference, Ref. [22, 23], because the finite-difference approximations are applied to the integrands in the energy integrals, rather than the differential equations of equilibrium. The program contains only isotropic hardening although both flow theory or deformation theory may be utilized. Secondary creep effects are also included. The solution scheme utilizes the tangent modulus method with Newton-Raphson iterations being performed in each cycle.

Numerical Integration

The only program using the numerical integration procedure for inelastic shell analysis to date was NONLEP, Ref. [24]. The program utilized Sanders shell theory, Ref. [25], and contained only isotropic hardening. There was no capability either for branched shell analysis or the solution of the coupled nonlinear torsion problem. The solution procedure for the nonlinear problem was Newton iteration. The newly available numerical integration program, STARS-2P, is the subject of this report, and its capabilities were briefly outlined in the introduction.

The comparative advantages and disadvantages of the three numerical approaches above were discussed in Ref. [26], and will not be repeated here. It should be noted, however, that the previous comments as to idealization grids should recieve even stronger emphasis in inelastic analysis, due to the

incremental nature of most solutions.

A final note on theory accuracy is also in order. The computational capability available for the inelastic analysis of shells has experienced a phenomenal growth recently, as exemplified by the programs discussed above. Indeed, the level of analysis capability that has been obtained has actually outstripped the ability to describe and verify complex material behavior such as cyclic, time and temperature dependent plasticity. The user of such programs must now be doubly on guard in using them in areas where the incorporated material behavior laws have not been verified by experiment.

CHAPTER 1

GENERAL NONLINEAR SHELL EQUATIONS

A full derivation of the pertinent equations may be found in Ref. [26] and [27]. For the axisymmetric small strain-moderate rotation case they are (see Fig. 1 for the geometry and sign conventions):

Strain-Displacement Relations

The nonlinear axisymmetric strain-displacement relations, for shells of revolution, are:

$$\begin{aligned} \epsilon_{\theta\theta} &= e_{\theta\theta} + \tfrac{1}{2}\omega_\varphi^2 \\ \epsilon_{\varphi\varphi} &= e_{\varphi\varphi} + \tfrac{1}{2}\omega_\theta^2 \\ \epsilon_{\zeta\zeta} &= \tfrac{1}{2}(\omega_\theta^2 + \omega_\varphi^2) \\ \epsilon_{\varphi\theta} &= \gamma_{\theta\varphi} - \omega_\theta\omega_\varphi \end{aligned} \tag{1}$$

where

$$\begin{aligned} e_{\theta\theta} &= e_{\theta\theta_0} - \zeta k_\theta \\ e_{\varphi\varphi} &= e_{\varphi\varphi_0} - \zeta k_\varphi \\ \gamma_{\theta\varphi} &= \gamma_{\theta\varphi_0} - 2\zeta k_{\theta\varphi} \end{aligned} \tag{2}$$

and

$$\begin{aligned} e_{\theta\theta_0} &= \frac{1}{r_0}\{v\cos\varphi - w\sin\varphi\} & k_\theta &= -\frac{1}{r_0}\{-\omega_\theta\cos\varphi\} \\ e_{\varphi\varphi_0} &= \frac{1}{r_1}\{v_{,\varphi} - w\} & k_\varphi &= \frac{1}{r_1}\omega_{\theta,\varphi} \\ \gamma_{\theta\varphi_0} &= \frac{1}{r_0}\{-u\cos\varphi\} + \frac{u_{,\varphi}}{r_1} & k_{\varphi\theta} &= \frac{1}{2r_0}\left\{-\frac{r_0}{r_1}\omega_{\varphi,\varphi} + \omega_\varphi\cos\varphi\right\} \end{aligned} \tag{3}$$

with ω_θ and ω_φ given by

$$\omega_\theta = \frac{1}{r_1}(w_{,\varphi} + v) \qquad \omega_\varphi = -\frac{1}{r_0}(u\sin\varphi) \tag{4}$$

Stress Resultant-Strain Relations

The stress-resultants are defined as (see Fig. 2 and 3 for sign convention):

$$N_\theta = \int \sigma_\theta d\zeta \qquad M_\theta = \int \sigma_\theta \zeta d\zeta$$

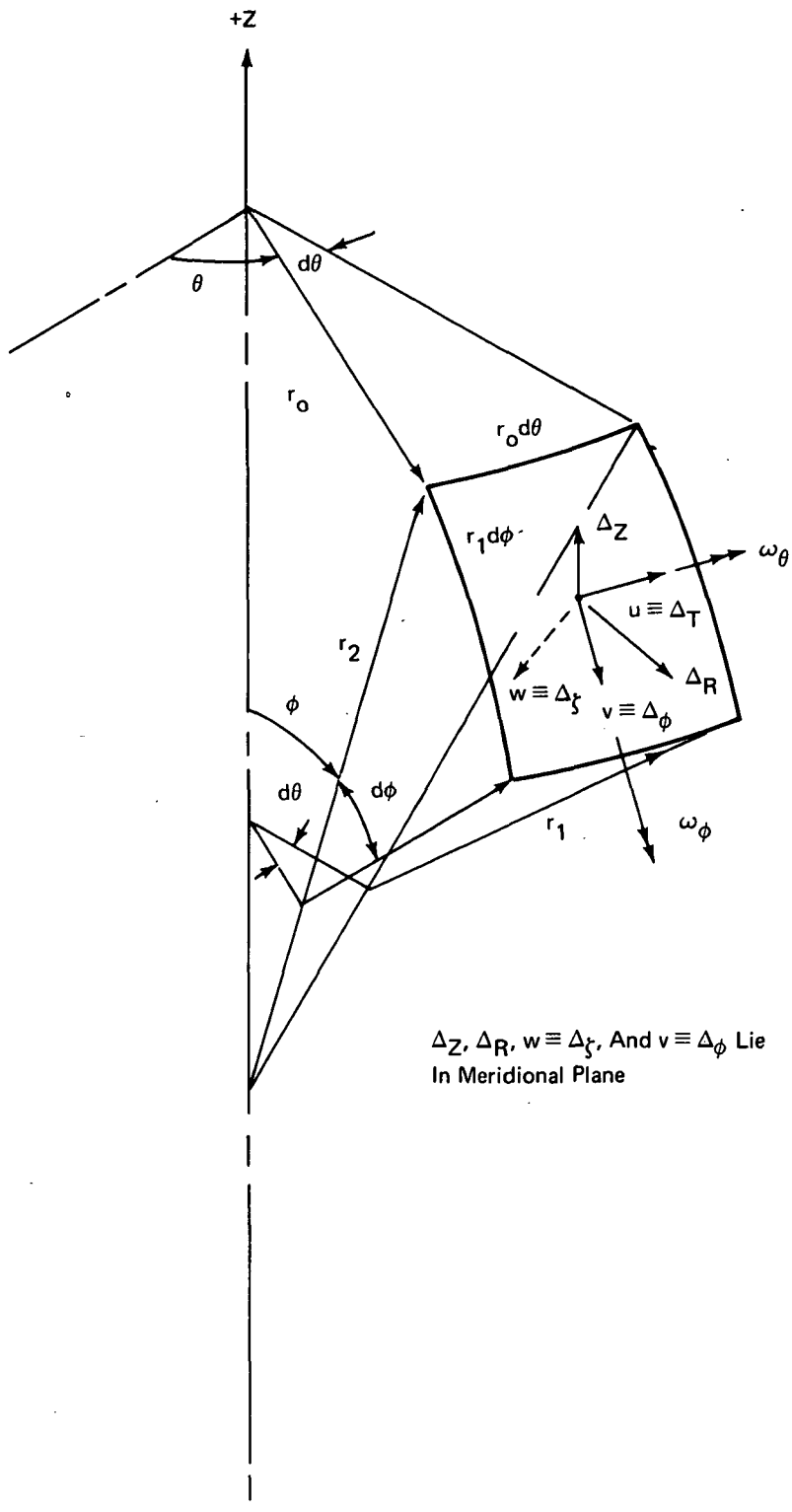

Fig. 1 Shell Geometry and Displacements

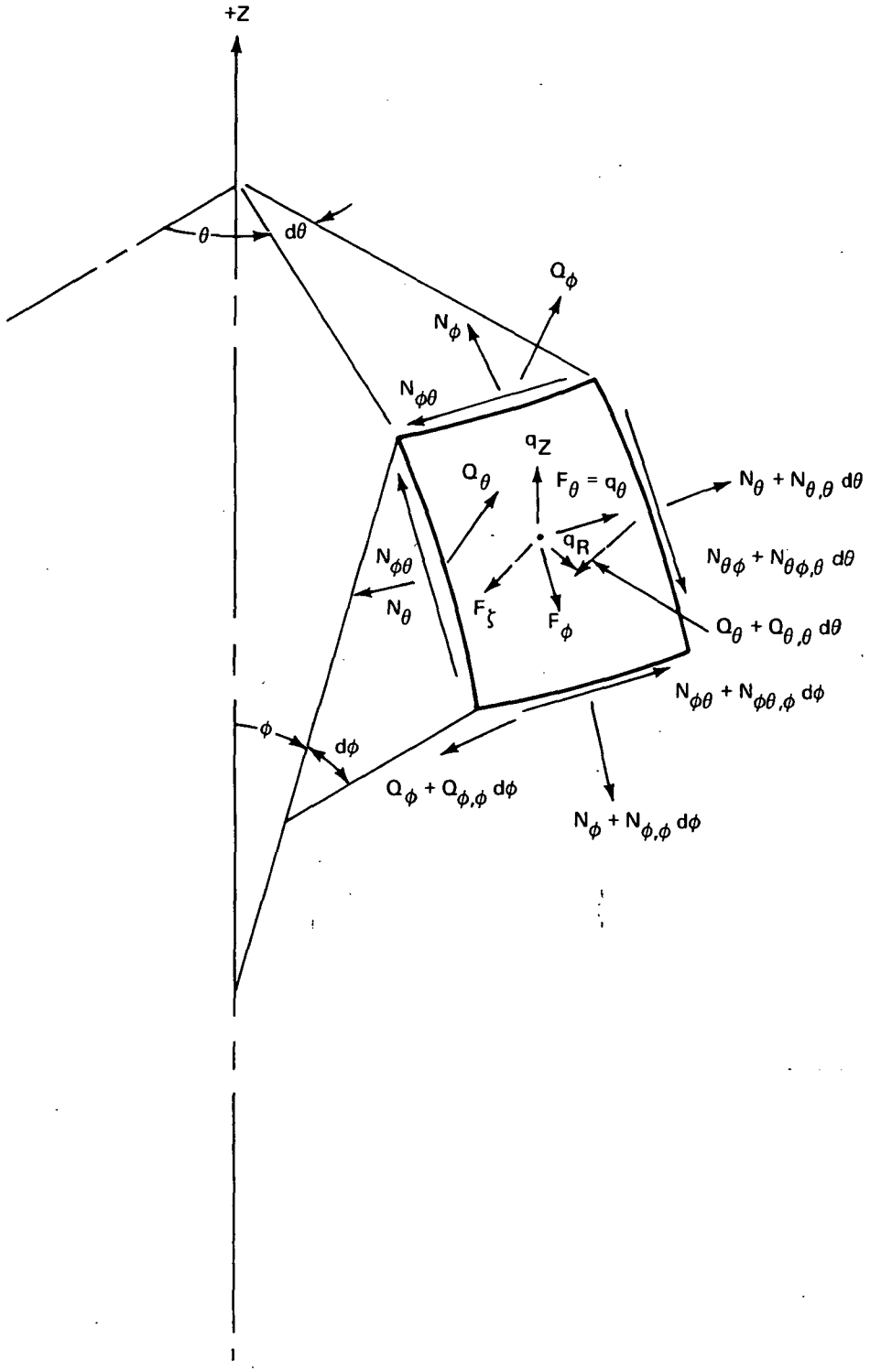

Fig. 2 Forces on Shell

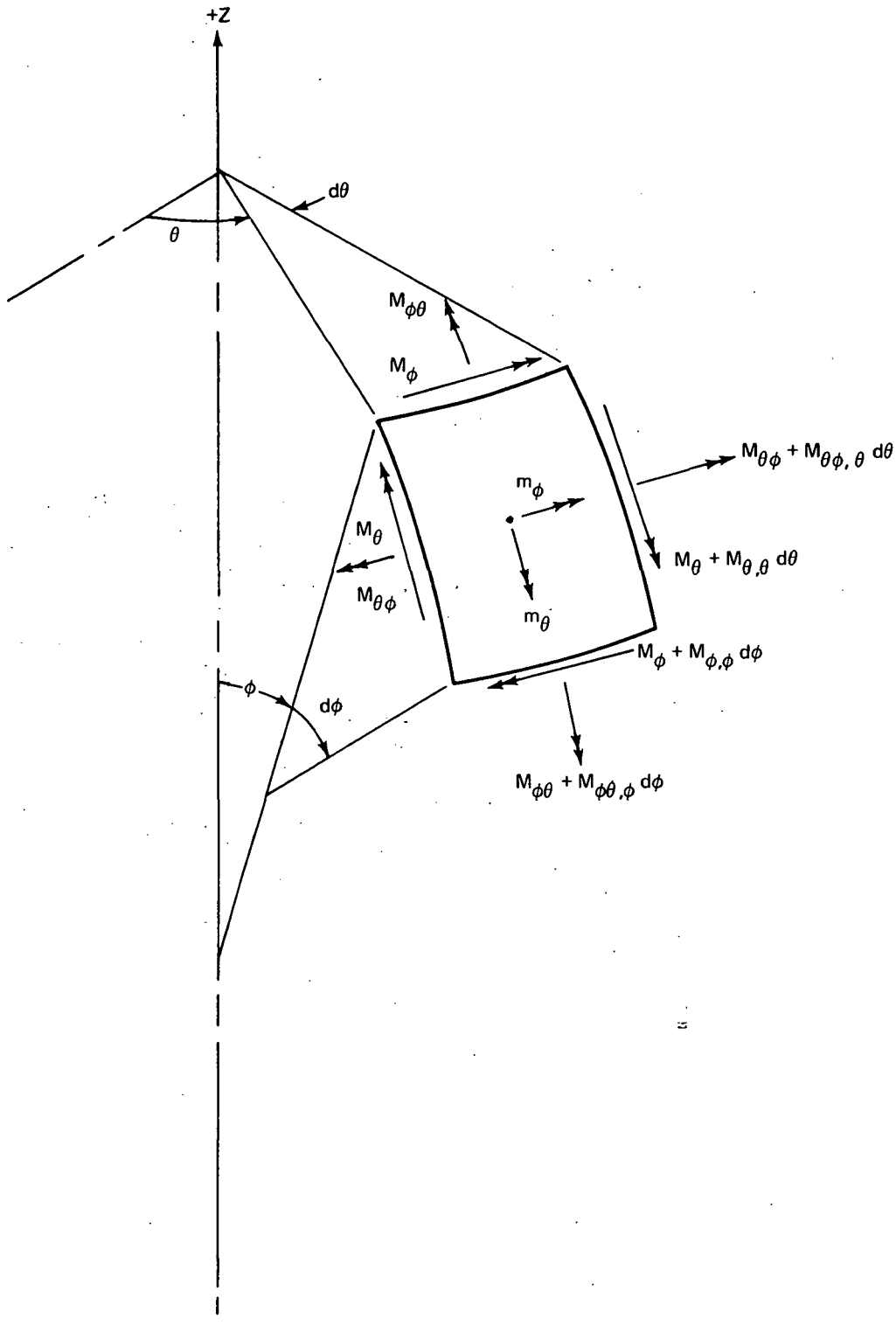

Fig. 3 Moments on Shell

$$N_\varphi = \int \sigma_\varphi \, d\zeta \qquad M_\varphi = \int \sigma_\varphi \zeta \, d\zeta$$

$$N_{\varphi\theta} = N_{\theta\varphi} = \int \tau_{\theta\varphi} d\zeta \qquad M_{\varphi\theta} = -M_{\theta\varphi} = \int \tau_{\theta\varphi} \zeta \, d\zeta \tag{5}$$

The thermal resultants are defined by

$$N_{T\theta} = \int \frac{E_\theta(\alpha_\theta + \nu_{\theta\varphi}\alpha_\varphi)T}{1 - \nu_{\varphi\theta}\nu_{\theta\varphi}} \, d\zeta \qquad M_{T\theta} = \frac{E_\theta(\alpha_\theta + \nu_{\theta\varphi}\alpha_\varphi)T}{1 - \nu_{\varphi\theta}\nu_{\theta\varphi}} \, \zeta d\zeta$$

$$N_{T\varphi} = \int \frac{E_\varphi(\alpha_\varphi + \nu_{\varphi\theta}\alpha_\theta)T}{1 - \nu_{\varphi\theta}\nu_{\theta\varphi}} \, d\zeta \qquad M_{T\varphi} = \int \frac{E_\varphi(\alpha_\varphi + \nu_{\varphi\theta}\alpha_\theta)T}{1 - \nu_{\varphi\theta}\nu_{\theta\varphi}} \, \zeta d\zeta \tag{6}$$

and the inelastic resultants are given by

$$\begin{Bmatrix} N_{I\theta} \\ M_{I\theta} \end{Bmatrix} = \int \frac{E_\theta(\epsilon_\theta^P + \nu_{\theta\varphi}\epsilon_\varphi^P)}{1 - \nu_{\varphi\theta}\nu_{\theta\varphi}} \begin{Bmatrix} 1 \\ \zeta \end{Bmatrix} d\zeta \,, \qquad \begin{Bmatrix} N_{I\varphi} \\ M_{I\varphi} \end{Bmatrix} = \int \frac{E_\varphi(\epsilon_\varphi^P + \nu_{\varphi\theta}\epsilon_\theta^P)}{1 - \nu_{\varphi\theta}\nu_{\theta\varphi}} \begin{Bmatrix} 1 \\ \zeta \end{Bmatrix} d\zeta$$

$$\begin{Bmatrix} N_{I\varphi\theta} \\ M_{I\varphi\theta} \end{Bmatrix} = \int G_{\varphi\theta}\gamma_{\theta\varphi}^P \begin{Bmatrix} 1 \\ \zeta \end{Bmatrix} d\zeta \tag{7}$$

where the superscript, P, indicates plastic strains.

Using the stress-strain relations for an orthotropic body in a state of plane stress, and using the centroidal surface as the reference surface of the shell wall, the stress-resultant strain expressions become:

$$N_\theta = K_{11}\left[e_{\theta\theta_0} + \nu_{\theta\varphi}\, e_{\varphi\varphi_0}\right] - N_{T\theta} - N_{I\theta}$$

$$N_\varphi = K_{22}\left[e_{\varphi\varphi_0} + \nu_{\varphi\theta} e_{\theta\theta_0}\right] - N_{T\varphi} - N_{I\varphi}$$

$$N_{\varphi\theta} = N_{\theta\varphi} = K_{33}\gamma_{\varphi\theta_0} - N_{I\varphi\theta} \tag{8}$$

$$M_\theta = -D_{11}\left[k_\theta + \nu_{\theta\varphi} k_\varphi\right] - M_{T\theta} - M_{I\theta}$$

$$M_\varphi = -D_{22}\left[k_\varphi + \nu_{\varphi\theta} k_\theta\right] - M_{T\varphi} - M_{I\varphi}$$

$$M_{\varphi\theta} = -M_{\theta\varphi} = -2D_{33}\, k_{\varphi\theta} - M_{I\varphi\theta}$$

Variations of the above equations may be obtained to account for different classes of smeared reinforcement, Ref. [26]. The definitions of the extensional stiffnesses K_{11}, K_{22}, bending stiffnesses D_{11}, D_{22}, and in-plane shear stiffnesses K_{33}, D_{33}, are available, for a variety of cross sections in Ref. [26].

Equilibrium Equations

The axisymmetric nonlinear equilibrium equations for shells of revolution are:

$$\frac{1}{r_0}\left(N_{\varphi\theta} r_0^2\right)_{,\varphi} - Q_\theta r_1 \sin\varphi = -r_1 r_0 (f_\theta^* + f_\theta)$$

$$
\begin{aligned}
&(N_\varphi r_0)_{,\varphi} - N_\theta r_1 \cos\varphi - r_0 Q_\varphi = -r_1 r_0 (f^*_\varphi + f_\varphi) \\
&(Q_\varphi r_0)_{,\varphi} + r_0 N_\varphi + N_\theta r_1 \sin\varphi = -r_1 r_0 (f^*_\zeta + f_\zeta) \\
&-(M_\varphi r_0)_{,\varphi} + M_\theta r_1 \cos\varphi + r_1 r_0 Q_\varphi = -r_1 r_0 m_\theta \\
&-(M_{\varphi\theta} r_0)_{,\varphi} - M_{\varphi\theta} r_1 \cos\varphi + r_1 r_0 Q_\theta = -r_1 r_0 m_\varphi \\
&N_{\theta\varphi} - N_{\varphi\theta} + \frac{M_{\theta\varphi}}{r_2} + \frac{M_{\varphi\theta}}{r_1} = 0
\end{aligned}
\tag{9}
$$

where

$$
\begin{aligned}
f^*_\theta &= \frac{1}{r_2}\left[N_\theta \omega_\varphi - N_{\varphi\theta}\omega_\theta\right] & f_\theta &= F_\theta(1 + e_{\theta\theta_0} + e_{\varphi\varphi_0}) + F_\varphi \frac{u_\varphi}{r_1} + F_\zeta \omega_\varphi \\
f^*_\varphi &= \frac{1}{r_2}\left[N_{\varphi\theta}\omega_\varphi - N_\varphi \omega_\theta\right] & f_\varphi &= F_\varphi(1 + e_{\theta\theta_0} + e_{\varphi\varphi_0}) - F_\zeta \omega_\theta \\
f^*_\zeta &= \frac{1}{r_0 r_1}\left\{r_0\left[N_\varphi \omega_\theta - N_{\varphi\theta}\omega_\varphi\right]\right\}_\varphi & f_\zeta &= F_\zeta(1 + e_{\theta\theta_0} + e_{\varphi\varphi_0}) - F_\theta \omega_\varphi + F_\varphi \omega_\theta
\end{aligned}
\tag{10}
$$

The f^*_i terms are the nonlinear contributions to the stiffness matrix (or they can be used, as shown, as effective geometric forces). The F_i terms are the applied surface forces tangential and normal to the deformed shell surface, the f_i are the forces in the undeformed coordinate system, and m_φ and m_θ are the distributed moments per unit surface area. It should be noted that the sixth equilibrium equation cannot in general be satisfied with this shell theory because of the assumption that $\zeta \ll r$. However, this equation is not employed in the subsequent solution of shell problems.

Boundary Conditions

On a φ = constant edge, we must have one of each of the following boundary conditions specified.

$$
\begin{aligned}
&u \quad \text{or} \quad T_{\varphi\theta} \\
&v \quad \text{or} \quad N_\varphi \\
&w \quad \text{or} \quad J^*_\varphi = Q_\varphi - r_1 f^*_\varphi \\
&\omega_\theta \quad \text{or} \quad M_\varphi
\end{aligned}
\tag{11}
$$

with the following definitions for the "Kirchoff-type" effective stress resultants:

$$
\begin{aligned}
T_{\varphi\theta} &= N_{\varphi\theta} - \frac{M_{\varphi\theta}}{r_0}\sin\varphi \\
J^*_\varphi &= Q_\varphi - N_{\varphi\theta}\omega_\varphi - N_\varphi \omega_\theta
\end{aligned}
\tag{12}
$$

Final Equations

These above equations for the axisymmetric case may be manipulated and put in the form of eight simultaneous first order differential equations in φ, convenient for use in a numerical integration computer code, Ref. [26]. For simple shell wall cross sections these are

$$\frac{T_{\varphi\theta,\varphi}}{r_1} = -2T_{\varphi\theta}\frac{\cos\varphi}{r_0} - M_{\varphi\theta}\frac{\cos\varphi}{r_0}\left[\frac{1}{r_1} - \frac{\sin\varphi}{r_0}\right] - f_\theta - m_\varphi\frac{\sin\varphi}{r_0}$$

$$- \frac{\sin\varphi}{r_0}\left[N_\theta\omega_\varphi - N_{\varphi\theta}\omega_\theta\right] \tag{13a}$$

$$\frac{N_{\varphi,\varphi}}{r_1} = -N_\varphi\frac{\cos\varphi}{r_0} + N_\theta\frac{\cos\varphi}{r_0} + \frac{J^*_\varphi}{r_1} - f_\varphi \tag{13b}$$

$$\frac{J^*_{\varphi,\varphi}}{r_1} = -J^*_\varphi\frac{\cos\varphi}{r_0} - N_\theta\frac{\sin\varphi}{r_0} - \frac{N_\varphi}{r_1} - f_\zeta \tag{13c}$$

$$\frac{M_{\varphi,\varphi}}{r_1} = M_\theta\frac{\cos\varphi}{r_0} - M_\varphi\frac{\cos\varphi}{r_0} + Q_\varphi + m_\theta \tag{13d}$$

$$\frac{u_{,\varphi}}{r_1} = u\frac{\cos\varphi}{r_0} + \frac{T_{\varphi\theta}}{K_{33}} + \frac{M_{\varphi\theta}}{r_0}\frac{\sin\varphi}{K_{33}} + \omega_\theta\omega_\varphi + \frac{N_{I\varphi\theta}}{K_{33}} \tag{13e}$$

$$\frac{v_{,\varphi}}{r_1} = \frac{w}{r_1} + (K_{22} - \nu^2_{\theta\varphi}K_{11})^{-1}\left\{N_\varphi - \nu_{\theta\varphi}N_\theta + (N_{T\varphi} + N_{I\varphi}) - \nu_{\theta\varphi}(N_{T\theta} + N_{I\theta})\right\} - \tfrac{1}{2}\omega^2_\theta \tag{13f}$$

$$\frac{w_{,\varphi}}{r_1} = \omega_\theta - \frac{v}{r_1} \tag{13g}$$

$$\frac{\omega_{\theta,\varphi}}{r_1} = (D_{22} - \nu^2_{\theta\varphi}D_{11})^{-1}\left\{-M_\varphi + \nu_{\theta\varphi}M_\theta - (M_{T\varphi} + M_{I\varphi}) + \nu_{\theta\varphi}(M_{T\theta} + M_{I\theta})\right\} \tag{13h}$$

$$N_\theta = \nu_{\varphi\theta}N_\varphi + (K_{11} - \nu^2_{\varphi\theta}K_{22})\left[\frac{v\cos\varphi - w\sin\varphi}{r_0} + \frac{1}{2}\omega^2_\varphi\right] - (N_{T\theta} + N_{I\theta}) + \nu_{\varphi\theta}(N_{T\varphi} + N_{I\varphi}) \tag{13i}$$

$$M_\theta = \nu_{\varphi\theta}M_\varphi - \frac{(D_{11} - \nu^2_{\varphi\theta}D_{22})}{r_0}\omega_\theta\cos\varphi - (M_{T\theta} + M_{I\theta}) + \nu_{\varphi\theta}(M_{T\varphi} + M_{I\varphi}) \tag{13j}$$

$$M_{\varphi\theta} = \left[\frac{-1}{\frac{r_0}{D_{33}} + \frac{\sin^2\varphi}{r_0K_{33}}}\right]\left\{u\left(\frac{\cos\varphi}{r_1} - \frac{\cos\varphi\sin\varphi}{r_0}\right) + \omega_\theta\omega_\varphi\sin\varphi\right.$$

$$\left. + \frac{T_{\varphi\theta}}{K_{33}}\sin\varphi + \frac{N_{I\varphi\theta}\sin\varphi}{K_{33}} - \frac{r_0M_{I\varphi\theta}}{D_{33}}\right\} \tag{13k}$$

$$Q_\varphi = J^*_\varphi + N_{\varphi\theta}\omega_\varphi - N_\varphi\omega_\theta$$

$$\omega_\varphi = -\frac{u\sin\varphi}{r_0} \tag{13m}$$

$$N_{\varphi\theta} = T_{\varphi\theta} + \frac{M_{\varphi\theta}}{r_0}\sin\varphi \tag{13n}$$

and

$$f_\theta = F_\theta\left(1 + \frac{v\cos\varphi - w\sin\varphi}{r_0} + \frac{1}{2}\omega_\varphi^2 + \frac{v_{,\varphi}}{r_1} - \frac{w}{r_1} + \frac{1}{2}\omega_\theta^2\right) + F_\varphi\frac{u_{,\varphi}}{r_1} + F_\zeta\omega_\varphi$$

$$f_\varphi = F_\varphi\left(1 + \frac{v\cos\varphi - w\sin\varphi}{r_0} + \frac{v_{,\varphi}}{r_1} - \frac{w}{r_1} + \frac{1}{2}\omega_\varphi^2 + \frac{1}{2}\omega_\theta^2\right) - F_\zeta\omega_\theta \tag{14}$$

$$f_\zeta = F_\zeta\left(1 + \frac{v\cos\varphi - w\sin\varphi}{r_0} + \frac{v_{,\varphi}}{r_1} - \frac{w}{r_1} + \frac{1}{2}\omega_\varphi^2 + \frac{1}{2}\omega_\theta^2\right) - F_\theta\omega_\varphi + F_\varphi\omega_\theta$$

For smeared reinforced wall cross sections more complicated sets of equations will arise, Ref. [26].

In order to apply the incremental Lagrangian approach, the typical variable in Eq. (13, 14) may be defined as

$$Y_{C_{i+1}} = Y_{C_i} + Y_\Delta \tag{15}$$

where Y_C is the converged value of a stress or displacement in equilibrium with a specific value of load, and Y_Δ is the increment necessary to accommodate an additional fraction of load. Since both $Y_{C_{i+1}}$ and Y_{C_i} must satisfy Eq. (13, 14), we may substitute Eq. (15) into Eq. (13, 14) and subtract the form of Eq. (13, 14) containing only Y_{C_i} to obtain the necessary differential equations which must be satisfied by Y_Δ. Performing this operation and further simplifying by neglecting nonlinear terms in Y_Δ, we can obtain the following incremental equations

$$\frac{T_{\varphi\theta,\varphi}}{r_1} = -2T_{\varphi\theta}\frac{\cos\varphi}{r_0} - M_{\varphi\theta}\frac{\cos\varphi}{r_0}\left[\frac{1}{r_1} - \frac{\sin\varphi}{r_0}\right] - f_\theta - m_\varphi\frac{\sin\varphi}{r_0}$$

$$-\frac{\sin\varphi}{r_0}\left[N_{\theta C_i}\omega_\varphi + N_\theta\omega_{\varphi C_i} - N_{\varphi\theta C_i}\omega_\theta - N_{\varphi\theta}\omega_{\theta C_i}\right] + R_1 \tag{16a}$$

$$\frac{N_{\varphi,\varphi}}{r_1} = -N_\varphi\frac{\cos\varphi}{r_0} + N_\theta\frac{\cos\varphi}{r_0} + \frac{J_\varphi^*}{r_1} - f_\varphi + R_2 \tag{16b}$$

$$\frac{J_{\varphi,\varphi}^*}{r_1} = -J_\varphi^*\frac{\cos\varphi}{r_0} - N_\theta\frac{\sin\varphi}{r_0} - \frac{N_\varphi}{r_1} - f_\zeta + R_3 \tag{16c}$$

$$\frac{M_{\varphi,\varphi}}{r_1} = M_\theta\frac{\cos\varphi}{r_0} - M_\varphi\frac{\cos\varphi}{r_0} + Q_\varphi + m_\theta + R_4 \tag{16d}$$

$$\frac{u_{,\varphi}}{r_1} = u\frac{\cos\varphi}{r_0} + \frac{T_{\varphi\theta}}{K_{33}} + \frac{M_{\varphi\theta}}{r_0}\frac{\sin\varphi}{K_{33}} + \omega_{\theta C_i}\omega_\varphi + \omega_\theta\omega_{\varphi C_i} + \frac{N_{I\varphi\theta}}{K_{33}} + R_5 \tag{16e}$$

$$\frac{v_{,\varphi}}{r_1} = \frac{w}{r_1} + (K_{22} - \nu_{\theta\varphi}^2 K_{11})^{-1}\{N_\varphi - \nu_{\theta\varphi}N_\theta + (N_{T\varphi} + N_{I\varphi}) - \nu_{\theta\varphi}(N_{T\theta} + N_{I\theta})\} - \omega_\theta\omega_{\theta C_i} + R_6 \tag{16f}$$

$$\frac{w_{,\varphi}}{r_1} = \omega_\theta - \frac{v}{r_1} \tag{16g}$$

$$\frac{\omega_{\theta,\varphi}}{r_1} = (D_{22} - \nu_{\theta\varphi}^2 D_{11})^{-1}\{-M_\varphi + \nu_{\theta\varphi} M_\theta - (M_{T\varphi} + M_{I\varphi}) + \nu_{\theta\varphi}(M_{T\theta} + M_{I\theta})\} + R_7 \tag{16h}$$

$$N_\theta = \nu_{\varphi\theta} N_\varphi + (K_{11} - \nu_{\varphi\theta}^2 K_{22})\left[\frac{v\cos\varphi - w\sin\varphi}{r_0} + \omega_\varphi \omega_{\varphi C_i}\right] - (N_{T\theta} + N_{I\theta}) + \nu_{\varphi\theta}(N_{T\varphi} + N_{I\varphi}) + R_8 \tag{16i}$$

$$M_\theta = \nu_{\varphi\theta} M_\varphi - \frac{(D_{11} - \nu_{\varphi\theta}^2 D_{22})}{r_0}\omega_\theta \cos\varphi - (M_{T\theta} + M_{I\theta}) + \nu_{\varphi\theta}(M_{T\varphi} + M_{I\varphi}) + R_9 \tag{16j}$$

$$M_{\varphi\theta} = \left[\frac{-1}{\frac{r_0}{D_{33}} + \frac{\sin^2\varphi}{r_0 K_{33}}}\right]\left\{u\left(\frac{\cos\varphi}{r_1} - \frac{\cos\varphi\sin\varphi}{r_0}\right) + \left(\omega_{\theta C_i}\omega_\varphi + \omega_\theta \omega_{\varphi C_i}\right)\sin\varphi \right.$$

$$\left. + \frac{T_{\varphi\theta}}{K_{33}}\sin\varphi + \frac{N_{I\varphi\theta}\sin\varphi}{K_{33}} - \frac{r_0 M_{I\varphi\theta}}{D_{33}}\right\} + R_{10} \tag{16k}$$

$$Q_\varphi = J_\varphi^* + N_{\varphi\theta_{C_i}}\omega_\varphi + N_{\varphi\theta}\omega_{\varphi C_i} - N_{\varphi C_i}\omega_\theta - N_\varphi \omega_{\theta C_i} \tag{16l}$$

$$\omega_\varphi = -\frac{u\sin\varphi}{r_0} \tag{16m}$$

$$N_{\varphi\theta} = T_{\varphi\theta} + \frac{M_{\varphi\theta}}{r_0}\sin\varphi \tag{16n}$$

and

$$f_\theta = F_\theta\left(1 + \frac{v_{C_i}\cos\varphi - w_{C_i}\sin\varphi}{r_0} + \frac{1}{2}\omega_{\varphi C_i}^2 + \frac{v_{C_i,\varphi}}{r_1} - \frac{w_{C_i}}{r_1} + \frac{1}{2}\omega_{\theta C_i}^2\right)$$

$$+ F_\varphi \frac{u_{C_i,\varphi}}{r_1} + F_\zeta \omega_{\varphi C_i} + F_{\theta C_i}\left(\frac{v\cos\varphi - w\sin\varphi}{r_0} + \frac{v_{,\varphi}}{r_1} - \frac{w}{r_1} + \omega_{\theta C_i}\omega_\theta + \omega_{\varphi C_i}\omega_\varphi\right) \tag{17a}$$

$$+ F_{\varphi C_i}\frac{u_{,\varphi}}{r_1} + F_{\zeta C_i}\omega_\varphi$$

$$f_\varphi = F_\varphi\left(1 + \frac{v_{C_i}\cos\varphi - w_{C_i}\sin\varphi}{r_0} + \frac{v_{C_i,\varphi}}{r_1} - \frac{w_{C_i}}{r_1} + \frac{1}{2}\omega_{\varphi C_i}^2 + \frac{1}{2}\omega_{\theta C_i}^2\right) - F_\zeta \omega_{\theta C_i}$$

$$+ F_{\varphi C_i}\left(\frac{v\cos\varphi - w\sin\varphi}{r_0} + \frac{v_{,\varphi}}{r_1} - \frac{w}{r_1} + \omega_{\theta C_i}\omega_\theta + \omega_{\varphi C_i}\omega_\varphi\right) - F_{\zeta C_i}\omega_\theta \tag{17b}$$

$$f_\zeta = F_\zeta\left(1 + \frac{v_{C_i}\cos\varphi - w_{C_i}\sin\varphi}{r_0} + \frac{v_{C_i,\varphi}}{r_1} - \frac{w_{C_i}}{r_1} + \frac{1}{2}\omega_{\varphi C_i}^2 + \frac{1}{2}\omega_{\theta C_i}^2\right) - F_\theta \omega_{\varphi C_i}$$

$$+ F_\varphi \omega_{\theta C_i} + F_{\zeta C_i}\left(\frac{v\cos\varphi - w\sin\varphi}{r_0} + \frac{v_{,\varphi}}{r_1} - \frac{w}{r_1} + \omega_{\theta C_i}\omega_\theta + \omega_{\varphi C_i}\omega_\varphi\right) - F_{\theta C_i}\omega_\varphi + F_{\varphi C_i}\omega_\theta \tag{17c}$$

In writing the above equation sets [Eq. (16, 17)] the subscript, Δ for incremental, has been omitted for

notational convenience. The R_i are remainder terms which will be discussed in the section describing equilibrium corrections (Chapter 3).

Equations (16) and (17) are the incremental equations which must be solved. Note that all the first order φ derivatives [Eq. (16a)–(16h)] are on natural boundary quantities, and that the equations contain previously accumulated stress and displacement quantities (subscript C_i).

CHAPTER 2

PLASTICITY ANALYSIS

This section considers appropriate incremental plasticity relations to determine values of stress and plastic strain developed during the history of loading. In STARS-2P, two hardening rules, kinematic hardening (see Fig. 5) and isotropic hardening (see Fig. 4), are available for initially isotropic, strain hardening materials. These are used in conjunction with the Von Mises yield condition. Drucker's postulate is used to obtain the associated flow rules. For initially orthotropic materials, only kinematic hardening theory is available for strain hardening materials. It is used in conjunction with Hill's orthotropic yield criterion, Ref. [28]. Ideally plastic behavior for initially isotropic or orthotropic materials may also be used. Additionally linear and nonlinear strain hardening capability is included in the program. Nonlinear hardening is achieved through use of the Ramberg-Osgood power law representation, Ref. [29], of the actual stress-strain data. A table of available plasticity options is presented in Fig. 6, while Fig. 7 illustrates how the input parameters determine which option is chosen. A detailed discussion of how plastic effects are included, the matrix plasticity relations, kinematic and isotropic hardening, and how to best choose material constants follows.

Inclusion of Plastic Effects in STARS

In STARS, plastic effects are incorporated using the "initial strain" concept, Ref. [30]. Plastic strains are interpreted to be initial strains present in the body in the same manner that thermal strains are treated. These initial strains are then applied as distributed "inelastic forces and moments." This effective load technique differs from the "tangent modulus" approach in which the actual structural material properties are adjusted to account for plastic effects. For the initial strain approach the additional assumption is made in the development of the governing differential equations [Eq. (13)-(14) of Chapter 1] that these initial strains are independent of the displacements. The increments of plastic strains (initial strains) are then calculated using subsidiary plastic relations (to be presented later). These plastic strain increments are then used to calculate the inelastic forces and moments N_I and M_I of Eq. (7).

As discussed in Chapters 1 and 3, an incremental predictor procedure is used to calculate the displacement increments for the current step. It is assumed that the initial strain increments used in the current step are those calculated at the end of the previous step. At the end of the current step an "equilibrium check" is made and any errors incurred in the prediction of plastic strains are adjusted through the application of the "equilibrium correction" in the differential equations, Eq. (16, 17).

To determine the inelastic forces and moments, the plastic strains are evaluated at each Runge-Kutta integration point at a specified number of layers through the thickness. For solid cross sections

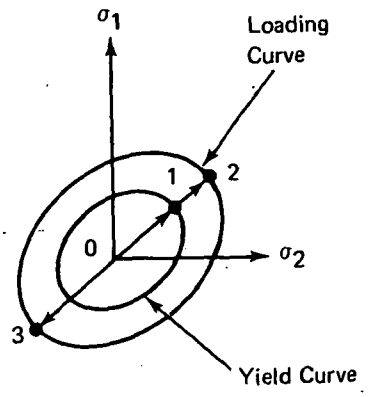

Fig. 4 Isotropic Hardening

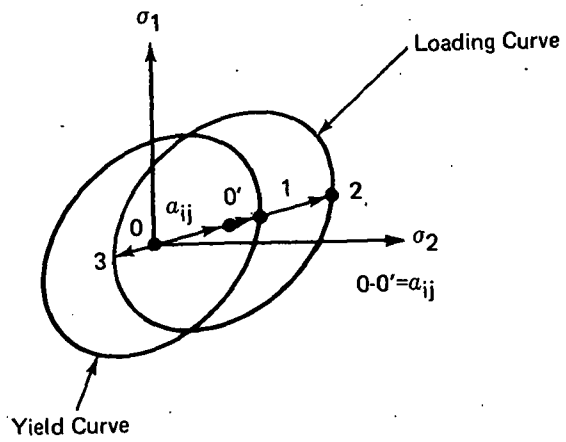

Fig. 5 Kinematic Hardening

Initial Material Behavior	Hardening Law	Available
Isotropic	Isotropic	Yes
	Kinematic	Yes
	Perfect Plasticity	Yes
Orthotropic	Isotropic	No
	Kinematic	Yes
	Perfect Plasticity	Yes

Note: Linear or nonlinear strain hardening is chosen on the basis of input plastic parameters.

Fig. 6 Available Plasticity Options

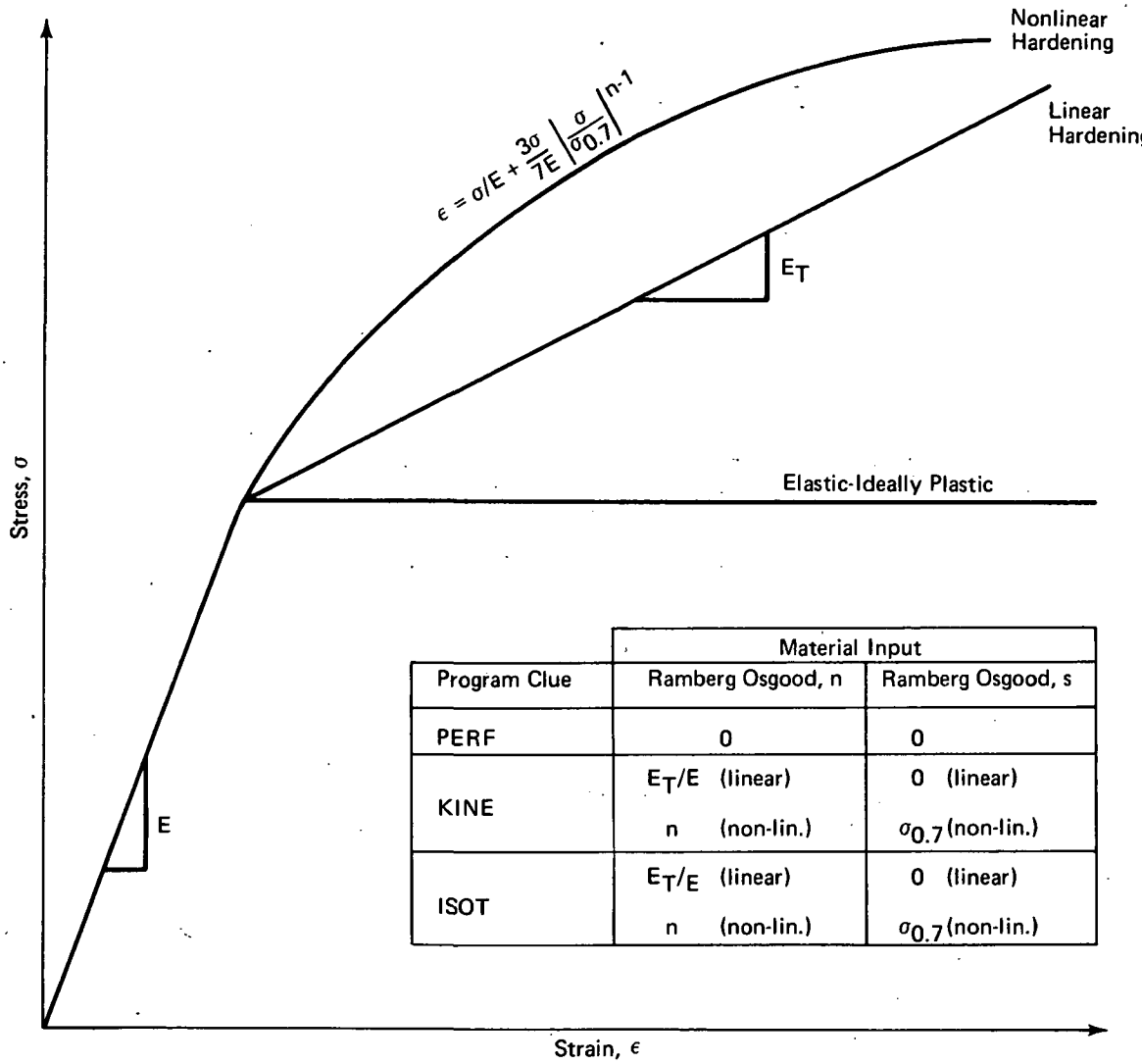

	Material Input	
Program Clue	Ramberg Osgood, n	Ramberg Osgood, s
PERF	0	0
KINE	E_T/E (linear)	0 (linear)
	n (non-lin.)	$\sigma_{0.7}$ (non-lin.)
ISOT	E_T/E (linear)	0 (linear)
	n (non-lin.)	$\sigma_{0.7}$ (non-lin.)

Fig. 7 Available Hardening Options

a maximum of 20 layers (21 integration points) through the thickness may be specified and the number of layers must be even. Ten layers is sufficient for most problems. For sandwich cross sections the maximum number of layers that can be specified is eight (nine integration points) and both top and bottom face sheets (even if they are unequal in thickness) will contain this number of layers. The incremental plastic forces and moments are then obtained by numerically integrating the plastic strains through the thickness using Simpson's rule, Ref. [31].

Matrix Relations-Strain Hardening

We can, for small strain increments, decompose the total strain increment $\{\Delta e^T\}$ into elastic $\{\Delta e^e\}$ and plastic $\{\Delta \epsilon^P\}$ components, as:

$$\{\Delta e^T\} = \{\Delta e^e\} + \{\Delta \epsilon^P\} \tag{18}$$

The elastic strain increments are related to the stress increments $\{\Delta\sigma\}$ by:

$$\{\Delta e^e\} = [E]^{-1}\{\Delta\sigma\} \tag{19}$$

where $[E]^{-1}$ is an array whose elements are combinations of elastic material constants. A linear incremental constitutive relation between plastic strains and stresses can be written for all of the popularly used flow theories of plasticity. This relationship can be expressed as:

$$\{\Delta \epsilon^P\} = [C]\{\Delta\sigma\} \tag{20}$$

Therefore, substituting Eq. (19) and (20) into (18) we can write:

$$\{\Delta\sigma\} = [R]^{-1}\{\Delta e^T\} \tag{21}$$

where $[R] = [E]^{-1} + [C]$.

The elements of the matrix [C] depend on the current state of stress, the yield condition, flow rule, and hardening law. In STARS the yield condition is based on Hill's yield criterion for an initially orthotropic material, Ref. [28], which reduces to the familiar Von Mises yield criterion for initially isotropic materials. The associated flow rule is based on Drucker's postulate, Ref. [32]. Two hardening laws are available. Prager-Ziegler kinematic hardening theory, Ref. [33, 34], is available for initially isotropic and initially orthotropic materials under cyclic loading. Isotropic hardening theory, Ref. [35], is available for only initially isotropic materials and is not suggested for cyclic loading situations because of its inability to predict the Bauschinger effect.

Both linear and nonlinear strain hardening rules may be used with either hardening law. Input parameters determine which law is chosen (see Fig. 7). To minimize the input requirements for nonlinear hardening, a Ramberg-Osgood, Ref. [29], representation of the stress-strain data is used:

$$\epsilon = \frac{\sigma}{E} + \frac{3\sigma}{7E}\left(\frac{\sigma}{\sigma_{0.7}}\right)^{n-1} \tag{22}$$

Thus for this representation of the stress-strain law, for an initially isotropic material two additional material parameters, n and $\sigma_{0.7}$, are required for the plastic analysis. For a Ramberg-Osgood representation of an initially orthotropic material these two quantities are required for each principal material direction and for each of the shear components. For a plane stress problem, as encountered in STARS, this means that three sets of stress-strain data must be specified (two for the normal components σ_φ, σ_θ, and one for the shear component $\tau_{\varphi\theta}$).

Kinematic Hardening

Kinematic hardening theory as presented by Prager and Ziegler, Ref. [33, 34], predicts a rigid body translation of the yield surface (see Fig. 5) without any expansion or rotation. It predicts an ideal Bauschinger effect and was originally derived for use with linear strain hardening. In fact, one of the unresolved questions in the use of the kinematic hardening theory of plasticity is the definition of the hardening coefficient, c, under multiaxial stress states. This is especially true for problems involving nonlinear hardening under cyclic loading. Several definitions have been proposed, Ref. [26, 27], with moderate success for initially isotropic behavior. An extension of this definition for initially orthotropic behavior based on Hill's yield criterion has been recently proposed, Ref. [38].

Before discussing the hardening coefficient, let us first rewrite the basic equations required for a plastic analysis using kinematic hardening.

First we need a yield condition, i.e., a rule to determine when plastic flow is initiated. In particular, let us use Hill's yield criterion for orthotropic materials:

$$f = F(\tilde{\sigma}_y - \tilde{\sigma}_z)^2 + G(\tilde{\sigma}_z - \tilde{\sigma}_x)^2 + H(\tilde{\sigma}_x - \tilde{\sigma}_y)^2 + 2L\tilde{\tau}_{yz}^2 + 2M\tilde{\tau}_{zx}^2 + 2N\tilde{\tau}_{xy}^2 = 1 \tag{23}$$

where

$$\frac{1}{X^2} = G + H \qquad \frac{1}{Y^2} = H + F \qquad \frac{1}{Z^2} = F + G$$

$$2L = \frac{1}{R^2} \qquad 2M = \frac{1}{S^2} \qquad 2N = \frac{1}{T^2}$$

Here $\tilde{\sigma}_{ij} = \sigma_{ij} - \alpha_{ij}$, with α_{ij} being the components of the shift in the yield surface, and X, Y, Z being the yield stresses in tension in the principal directions of orthotropy, and R, S, T being the yield stresses in shear with respect to the principal axes. For initially isotropic materials this reduces to the familiar Von Mises yield condition:

$$f = \left(\frac{\tilde{\sigma}_x - \tilde{\sigma}_y}{2}\right)^2 + \left(\frac{\tilde{\sigma}_y - \tilde{\sigma}_z}{2}\right)^2 + \left(\frac{\tilde{\sigma}_z - \tilde{\sigma}_x}{2}\right)^2 + 3\tilde{\tau}_{xy}^2 + 3\tilde{\tau}_{yz}^2 + 3\tilde{\tau}_{zx}^2 = \sigma_0^2 \tag{24}$$

with σ_0 equal to the initial yield stress in tension.

Stability requirements for the use of Hill's form of the yield surface, i.e., insuring that it remain a "closed ellipsoidal" surface, require that the following criterion must also be satisfied by the yield stresses, Ref. [39];

$$F_{11}F_{22} - F_{12}^2 = 0 \tag{25}$$

where

$$F_{11} = \frac{1}{X^2} \qquad F_{22} = \frac{1}{Y^2} \qquad F_{12} = -\frac{1}{2}\left(\frac{1}{X^2} + \frac{1}{Y^2} - \frac{1}{Z^2}\right)$$

If Eq. (25) is not satisfied by the yield stresses then some other yield criterion must be chosen (see Ref. [39] for example) and implemented in the code.

The associated flow rule used in STARS-2P is based on Drucker's postulate:

$$d\epsilon_{ij}^P = d\lambda \frac{\partial f}{\partial \sigma_{ij}} \tag{26}$$

where $d\lambda$ is a positive scalor quantity. For kinematic hardening it is given by:

$$d\lambda = \frac{1}{c} \frac{\frac{\partial f}{\partial \sigma_{mn}} d\sigma_{mn}}{\left(\frac{\partial f}{\partial \sigma_{kl}}\right)\left(\frac{\partial f}{\partial \sigma_{kl}}\right)} \tag{27}$$

and c is the hardening coefficient to be defined. The incremental shift in the yield surface $d\alpha_{ij}$ is assumed to be along a radial line through the center of the yield surface as postulated by Ziegler, Ref. [34]:

$$d\alpha_{ij} = d\mu(\sigma_{ij} - \alpha_{ij}) \tag{28}$$

and

$$d\mu = \frac{\frac{\partial f}{\partial \sigma_{ij}} d\sigma_{ij}}{(\sigma_{ij} - \alpha_{ij}) \frac{\partial f}{\partial \sigma_{ij}}} \tag{29}$$

In evaluating the terms of Eq. (26)–(29) for subsets of the nine dimensional stress space, all stress terms are retained in the yield function. Symmetry is applied, as well as setting stresses identically equal to zero, after the expressions for $d\lambda$ and $d\mu$ have been obtained. This is termed complete kinematic hardening.

For plane stress kinematic hardening the appropriate terms for the relationship between plastic strain and stress increments given by Eq. (20) are

$$\{\Delta\epsilon^P\}=\begin{Bmatrix}\Delta\epsilon_\varphi^P\\ \Delta\epsilon_\theta^P\\ \Delta\gamma_{\varphi\theta}^P\end{Bmatrix} \qquad \{\Delta\sigma\}=\begin{Bmatrix}\Delta\sigma_\varphi\\ \Delta\sigma_\theta\\ \Delta\tau_{\varphi\theta}\end{Bmatrix}$$

$$[C]=\frac{1}{D}\begin{bmatrix}M_1^2 & M_1M_2 & M_1M_3\\ M_2M_1 & M_2^2 & M_2M_3\\ M_3M_1 & M_3M_2 & M_3^2\end{bmatrix} \qquad D=c\left(M_1^2+M_2^2+\frac{M_3^2}{2}+M_4^2\right) \tag{30}$$

where

$$M_1=2(G+H)\tilde{\sigma}_\varphi-2H\tilde{\sigma}_\theta \qquad M_2=2(F+H)\tilde{\sigma}_\theta-2H\tilde{\sigma}_\varphi$$

$$M_3=4N\tilde{\tau}_{\varphi\theta} \qquad M_4=-2F\tilde{\sigma}_\theta-2G\tilde{\sigma}_\varphi$$

and the expression used to obtain the $\Delta\alpha_{ij}$ from Eq. (28, 29) is

$$\begin{Bmatrix}\Delta\alpha_\varphi\\ \Delta\alpha_\theta\\ \Delta\alpha_{\varphi\theta}\end{Bmatrix}=\frac{M_1\Delta\sigma_\varphi+M_2\Delta\sigma_\theta+M_3\Delta\tau_{\varphi\theta}}{2}\begin{Bmatrix}\sigma_\varphi-\alpha_\varphi\\ \sigma_\theta-\alpha_\theta\\ \tau_{\varphi\theta}-\alpha_{\varphi\theta}\end{Bmatrix}$$

There still remains the problem of determining c, the hardening coefficient. If we evaluate c for a uniaxial state of stress and restrict ourselves to initially isotropic materials, using Eq. (26), (27), and (24), we get:

$$\frac{1}{c}=\frac{3}{2}\frac{d\epsilon^P}{d\sigma} \tag{31}$$

If we generalize to a multiaxial state of stress, we may consider σ and ϵ^P to be effective quantities $\bar{\sigma}$ and $\bar{\epsilon}^P$, Ref. [36], where for an initially isotropic material

$$\bar{\sigma}^2=\left(\frac{\sigma_x-\sigma_y}{2}\right)^2+\left(\frac{\sigma_y-\sigma_z}{2}\right)^2+\left(\frac{\sigma_z-\sigma_x}{2}\right)^2+3\tau_{yz}^2+3\tau_{zx}^2+3\tau_{xy}^2 \tag{32}$$

and

$$d\bar{\epsilon}^P=\sqrt{(2/3)d\epsilon_{ij}^P d\epsilon_{ij}^P}$$

Note the difference in the definition of the "effective stress" $\bar{\sigma}$ and the yield function "f" of Eq. (24).

If we use a Ramberg-Osgood representation of the stress-strain curve and consider the nonlinear term to represent the plastic strain contribution, then:

$$\frac{1}{c} = \frac{3}{2}\frac{d\bar{\epsilon}^P}{d\bar{\sigma}} = \frac{3}{2}\left(\frac{3n}{7E}\left|\frac{\bar{\sigma}}{\sigma_{0.7}}\right|^{n-1}\right) \tag{33}$$

or for linear strain hardening

$$\frac{1}{c} = \frac{3}{2}\frac{d\bar{\epsilon}^P}{d\bar{\sigma}} = \frac{3}{2}\left[\frac{1}{E}\,\frac{\left(1-\frac{E_T}{E}\right)}{E_T/E}\right] \tag{34}$$

where E_T is the tangent modulus.

Various methods of choosing an appropriate value for E_T/E from a stress-strain curve have been suggested (see Ref. [40] for example). The use of linear strain hardening can lead to substantial underprediction of plastic strains in the range of strain where the material does not have a linear stress-plastic strain relationship. In turn this can lead to serious discrepancies if the response to cyclic loading is desired.

To determine the values of n and $\sigma_{0.7}$ that best fit the actual stress-strain data, the method suggested by Ramberg and Osgood can be used if the strain range is sufficiently small. For this case

$$n = 1 + \frac{\log(17/7)}{\log(\sigma_{0.7}/\sigma_{0.85})}$$

The quantities $\sigma_{0.7}$ and $\sigma_{0.85}$ are the stresses at which the curve has secant moduli of 0.7E and 0.85E, respectively. If the strain of interest is sufficiently large so that the parameters as determined by the preceding process do not fit the curve well, then a power law representation to fit the actual data can be used

$$\epsilon = \frac{\sigma}{E} + \beta\sigma^n \tag{35}$$

Now having determined β and n to "best fit" the experimental data, the value of n input is that calculated, and the value of $\sigma_{0.7}$ input is gotten by equating the nonlinear terms of Eq. (35) and (33), i.e.,

$$\sigma_{0.7} = \left(\frac{3}{7E\beta}\right)^{\frac{1}{n-1}} \tag{36}$$

For cyclic loading the problem of how to determine c for load reversals subsequent to the initial loading is even more vexing expecially for nonlinear hardening. For linear hardening a procedure for selecting the value of c and new yield stresses for succeeding cycles is suggested in Ref. [40]. For nonlinear hardening it is desirable to reproduce the actual hysteretic stress-strain curves obtained

from test data. Morrow, Ref. [41], details extensive cyclic tests on isotropic metals to determine the cyclic and hysteresis stress-strain curves. He has found that both the cyclic and hysteresis curves may be well represented by a power law similar to the Ramberg-Osgood curves. Based on his findings, we have incorporated into STARS-2P a hardening coefficient for load reversals following the initial monotonic loading defined as:

$$\frac{1}{c} = \frac{3}{2}\frac{d\bar{\epsilon}^P}{d\bar{\sigma}} = \frac{3}{2}\left[\frac{3n}{7E}\left|\frac{\bar{\sigma}}{2\sigma_{0.7}}\right|^{n-1}\right] \tag{37}$$

where we now define $\bar{\sigma}$ to be

$$\bar{\sigma}^2 = \left(\frac{\sigma_x^* - \sigma_y^*}{2}\right)^2 + \left(\frac{\sigma_y^* - \sigma_z^*}{2}\right)^2 + \left(\frac{\sigma_z^* - \sigma_x^*}{2}\right)^2 + 3\tau_{xy}^{*2} + 3\tau_{yz}^{*2} + 3\tau_{zx}^{*2} \tag{38}$$

where $\sigma_{ij}^* = \sigma_{ij} - \hat{\sigma}_{ij}$, and $\hat{\sigma}_{ij}$ is the last value of stress at the end of the previous loading range.

A generalization of the definition of c for initially orthotropic materials based on Hill's yield criterion is presented in Ref. [38]. The basic highlights will be reproduced here.

We define c, for plane stress, to be:

$$\frac{1}{c} = \frac{1}{c_\varphi}\frac{\frac{\partial f}{\partial \sigma_\varphi}\bar{\sigma}_\varphi}{2f} + \frac{1}{c_\theta}\frac{\frac{\partial f}{\partial \sigma_\theta}\bar{\sigma}_\theta}{2f} + \frac{1}{c_{\varphi\theta}}\frac{\frac{\partial f}{\partial \tau_{\varphi\theta}}\bar{\tau}_{\varphi\theta}}{2f}$$

where (39)

$$c_\varphi = \frac{(G+H)^2}{[(G+H)^2 + H^2 + G^2]}\frac{d\sigma_\varphi}{d\epsilon_\varphi^P}$$

$$c_\theta = \frac{(F+H)^2}{[(F+H)^2 + H^2 + F^2]}\frac{d\sigma_\theta}{d\epsilon_\theta^P}$$

$$c_{\varphi\theta} = 2\frac{d\tau_{\varphi\theta}}{d\gamma_{\varphi\theta}^P}$$

This form for c reduces to the individual uniaxial stress-strain laws and the initially isotropic case given in Eq. (31).

For a linear strain hardening approximation, we use:

$$\frac{d\epsilon_\varphi^P}{d\sigma_\varphi} = \frac{1}{E_\varphi}\frac{(1 - E_{T_\varphi}/E_\varphi)}{(E_{T_\varphi}/E_\varphi)}; \qquad \frac{d\epsilon_\theta^P}{d\sigma_\theta} = \frac{1}{E_\theta}\frac{(1 - E_{T_\theta}/E_\theta)}{(E_{T_\theta}/E_\theta)}$$

$$\frac{d\gamma_{\varphi\theta}^P}{d\tau_{\varphi\theta}} = \frac{1}{G_{\varphi\theta}}\frac{(1 - G_{T_{\varphi\theta}}/G_{\varphi\theta})}{(G_{T_{\varphi\theta}}/G_{\varphi\theta})} \tag{40}$$

where E_{T_φ}, E_{T_θ} and $G_{T_{\varphi\theta}}$ are specified by the user for each component direction.

For a Ramberg-Osgood form of the uniaxial stress-strain data we use:

$$\frac{d\epsilon_\varphi^P}{d\sigma_\varphi} = \frac{3n_\varphi}{7E_\varphi}\left[\frac{\sqrt{2/3\dfrac{(F+G+H)}{G+H}}\,\bar{\sigma}^2}{\sigma_{0.7\varphi}}\right]^{n_\varphi-1}$$

$$\frac{d\epsilon_\theta^P}{d\sigma_\theta} = \frac{3n_\theta}{7E_\theta}\left[\frac{\sqrt{2/3\dfrac{(F+G+H)}{F+H}}\,\bar{\sigma}^2}{\sigma_{0.7\theta}}\right]^{n_\theta-1} \tag{41}$$

$$\frac{d\gamma_{\varphi\theta}^P}{d\tau_{\varphi\theta}} = \frac{3n_{\varphi\theta}}{7G_{\varphi\theta}}\left[\frac{\sqrt{2/3\dfrac{(F+G+H)}{2N}}\,\bar{\sigma}^2}{\tau_{0.7\varphi\theta}}\right]^{n_{\varphi\theta}-1}$$

where we have defined the effective stress $\bar{\sigma}$ (for a full three-dimensional stress space) to be:

$$\bar{\sigma}^2 = \frac{3}{2(F+G+H)}\left[F(\sigma_y-\sigma_z)^2 + G(\sigma_z-\sigma_x)^2 + H(\sigma_x-\sigma_y)^2 + 2L\tau_{yz}^2 + 2M\tau_{zx}^2 + 2N\tau_{xy}^2\right] \tag{42}$$

for initially orthotropic materials. For plane stress, x corresponds to φ, y to θ, and all stresses with subscript z are zero.

Now for plane stress, n_φ, $\sigma_{0.7_\varphi}$, n_θ, $\sigma_{0.7_\theta}$, $n_{\varphi\theta}$, and $\tau_{0.7_{\varphi\theta}}$ are specified by the user for each component direction.

For cyclic loading we specify $\bar{\sigma}$ to be:

$$\bar{\sigma}^2 = \frac{3}{2(F+G+H)}\left[F(\sigma_y^*-\sigma_z^*)^2 + G(\sigma_z^*-\sigma_x^*)^2 + H(\sigma_x^*-\sigma_y^*)^2 + 2L\tau_{yz}^{*2} + 2M\tau_{zx}^{*2} + 2N\tau_{xy}^{*2}\right] \tag{43}$$

where $\sigma_{ij}^* = \sigma_{ij} - \hat{\sigma}_{ij}$.

Data for orthotropic cyclic loading is seriously lacking. If the representation given by Eqs. (39, 41, 43) is deemed valid, then $\sigma_{0.7_{ij}}$ should be set to twice the measured monotonic value for load reversals after the initial loading range. Additionally at the end of each half cycle of loading new plastic material properties may be input so that each hysteresis loop may be accurately represented.

At times, due to nonproportional loading or other reasons, local unloading occurs even though the applied load is increasing. The unloading criterion, which is checked in the program for every load increment, is given by

$$\frac{\partial f}{\partial \sigma_{ij}} d\sigma_{ij} \geq 0 \quad \text{for loading or neutral loading}$$

$$\frac{\partial f}{\partial \sigma_{ij}} d\sigma_{ij} < 0 \quad \text{for unloading}$$

For plane stress kinematic hardening, this is given by:

$$(\bar{\sigma}_\varphi - \tfrac{1}{2}\bar{\sigma}_\theta)d\sigma_\varphi + (\bar{\sigma}_\theta - \tfrac{1}{2}\bar{\sigma}_\varphi)d\sigma_\theta + 3\bar{\tau}_{\varphi\theta}d\tau_{\varphi\theta} < 0 \tag{44}$$

for initially isotropic materials, and by

$$[(G+H)\bar{\sigma}_\varphi - H\bar{\sigma}_\theta]d\sigma_\varphi + [(F+H)\bar{\sigma}_\theta - H\bar{\sigma}_\varphi]d\sigma_\theta + 2N\bar{\tau}_{\varphi\theta}d\tau_{\varphi\theta} < 0 \tag{45}$$

for initially orthotropic materials. The values of $d\sigma_{ij}$ used are obtained from the "elastic" stress-strain relations for that increment. They are the actual $d\sigma_{ij}$ if unloading is detected, and are neglected if continued loading occurs. For continued loading the actual $d\sigma_{ij}$ are determined from the plasticity relations. If unloading is detected at a point, then all further stress and strain increments are elastic until reloading is detected using the appropriate yield criterion.

Isotropic Hardening

Isotropic hardening theory assumes that during plastic flow the loading surface expands uniformly about the origin in stress space, maintaining the same shape, center location, and orientation as the yield surface (see Fig. 4). This representation of work hardening does not account for the Bauschinger effect exhibited by most structural materials. In fact, this theory provides that because of work hardening the material will exhibit an increase in the compressive yield stress equal to the increase in the tensile yield stress. For monotonic loading conditions, however, isotropic hardening is satisfactory and is commonly used. In STARS-2P it may only be used with initially isotropic materials.

The yield condition is the Von Mises yield condition given by Eq. (24) with the α_{ij} equal to zero. Now σ_0 increases in magnitude to provide for expansion of the yield surface. For isotropic hardening, σ_0 may be defined by Eq. (24) to be the "effective stress, $\bar{\sigma}$." The flow rule is again given by Drucker's postulate [see Eq. (26)].

For isotropic hardening we can show:

$$d\lambda = \tfrac{1}{2}\frac{d\bar{\sigma}}{\bar{\sigma}H'} \tag{46}$$

where $H' = d\bar{\sigma}/d\bar{\epsilon}^p$ or the slope of the effective stress effective plastic strain curve. Also:

$$d\bar{\sigma} = \frac{(\sigma_\varphi - \tfrac{1}{2}\sigma_\theta)d\sigma_\varphi + (\sigma_\theta - \tfrac{1}{2}\sigma_\varphi)d\sigma_\theta + 3\tau_{\varphi\theta}d\tau_{\varphi\theta}}{\bar{\sigma}}$$

for plane stress. Here $\bar{\sigma}^2 = \sigma_\varphi^2 - \sigma_\varphi\sigma_\theta + \sigma_\theta^2 + 3\tau_{\varphi\theta}^2$. We can then write the elements of [C] as:

$$[C] = \frac{1}{D}\begin{bmatrix} M_1^2 & M_1M_2 & M_1M_3 \\ M_1M_2 & M_2^2 & M_2M_3 \\ M_1M_3 & M_2M_3 & M_3^2 \end{bmatrix} \tag{47}$$

and

$$D = \bar{\sigma}^2 H'$$

where

$$M_1 = \sigma_\varphi - \tfrac{1}{2}\sigma_\theta \ , \quad M_2 = \sigma_\theta - \tfrac{1}{2}\sigma_\varphi \ , \quad M_3 = 3\tau_{\varphi\theta}$$

These relations may be used with linear or nonlinear strain hardening laws as described in the section on kinematic hardening. Again the input consists of the value E_T/E for linear strain hardening or n and $\sigma_{0.7}$ for a Ramberg-Osgood representation of nonlinear strain hardening. It is not recommended that isotropic hardening be used for problems involving cyclic loading with stress reversals in the plastic range. If one wanted to do so, however, the plastic material properties may be changed at the end of each half cycle of loading.

Local unloading is detected in a manner similar to that described in the section on kinematic hardening, i.e.,

$$\frac{\partial f}{\partial \sigma_{ij}} d\sigma_{ij} < 0 \quad \text{for unloading} \tag{48}$$

For plane stress isotropic hardening, this is given by

$$(\sigma_\varphi - \tfrac{1}{2}\sigma_\theta)d\sigma_\varphi + (\sigma_\theta - \tfrac{1}{2}\sigma_\varphi)d\sigma_\theta + 3\tau_{\varphi\theta}d\tau_{\varphi\theta} < 0 \tag{49}$$

where the values of $d\sigma_{ij}$ used are the potential elastic stress increments for that step. Again they are the actual $d\sigma_{ij}$ if unloading is detected and meaningless if continued loading occurs. This unloading criterion is identical to that used by Yamada et al., Ref. [42].

Matrix Relations—Perfect Plasticity

The treatment of multiaxial elastic ideally plastic behavior requires that the following conditions be satisfied:

- The stress increment vector must be tangent to the loading surface.
- The plastic strain increment vector must be normal to the loading surface, where the loading surface is the representation in stress space of the initial yield function or the subsequent yield function after some plastic deformation has occurred.

If $f(\sigma_{ij})$ represents the yield surface, the first condition can be expressed analytically as:

$$\frac{\partial f}{\partial \sigma_{ij}} d\sigma_{ij} = 0 \tag{50}$$

and provides a linear relationship among the components of stress increment. Thus, one of the com-

ponents may be expressed in terms of the others. In matrix form, this can be written as:

$$\{\Delta\sigma\} = [\underset{\sim}{E}]\{\underline{\Delta\sigma}\} \tag{51}$$

where $\{\underline{\Delta\sigma}\}$ represents the independent stress components.

The normality condition provides a linear relation among the various components of the plastic strain increment

$$d\epsilon^P_{ij} = d\lambda \frac{\partial f}{\partial \sigma_{ij}} \tag{52}$$

This condition is derived from the flow rule and provides a linear relationship in which each of the components of plastic strain increment can be written in terms of any one component. This relationship may be represented in the following form:

$$\{\Delta\epsilon^P\} = [\underset{\sim}{E}]\{\underset{\sim}{\Delta}\epsilon^P\} \tag{53}$$

where $\{\underset{\sim}{\Delta}\epsilon^P\}$ is the independent plastic strain increment.

It is apparent from Eqs. (51) and (53) that the independent increments of stress and plastic strain can be combined and written in the components of a vector, $\{\Delta\omega\}$ (see Ref. [36]) so that Eqs. (51, 53) can be written, respectively, as:

$$\{\Delta\sigma\} = [\underset{\sim}{E}]\{\Delta\omega\} \tag{54}$$

$$\{\Delta\epsilon^P\} = [\underset{\sim}{E}]\{\Delta\omega\} \tag{55}$$

Combining the above equations with Eqs. (18) and (19), we can form the following relation for the independent quantities:

$$\{\Delta\omega\} = [E^*]^{-1}\{\Delta e^T\} \tag{56}$$

where $[E^*] = [E]^{-1}[\underset{\sim}{E}] + [\underset{\sim}{E}]$.

These relations are used with Hill's yield criterion [Eq. (18)] for initially orthotropic behavior which reduces to the Von Mises yield criterion for initially isotropic materials. Ideally plastic behavior is specified in STARS-2P by zero n and $\sigma_{0.7}$ on the material property cards. For initially orthotropic materials either <u>all</u> components of the stress-strain law must be ideally plastic or <u>none</u> must be.

CHAPTER 3

NUMERICAL SOLUTION PROCEDURE

The matrix solution procedure utilized in the STARS-2P program is basically that of Ref. [26], and thus will only be briefly outlined here. More detail will be expended in discussing the specialized requirements created by the plasticity analysis; namely the plastic incremental load vector, and equilibrium corrections in an incremental analysis.

The basic steps in the STARS numerical solution procedure can be outlined as follows:

(i) For a numerical integration procedure, a segment length must be chosen. This is defined as the length along a shell meridian where numerical integration can proceed without encountering any small differences of large numbers in the subsequent matrix formulation. The differential equations, Eq. (16-17) are first integrated by the Runge-Kutta procedure, for each shell segment. Eight initial vectors are used on the homogeneous equations (Eq. (16-17)) with $f_i = N_{Ti} = M_{Ti} = N_{Ii} = M_{Ii} = R_i \equiv 0$), wherein each natural boundary quantity is set alternately to unity with all others being zero. A final integration with all zero initial conditions is performed on Eq. (16-17), but now including all the load terms.

(ii) The above integrations give rise to the following influence coefficient matrix equations between the incremental shell forces, F, displacements, Δ, and loading, ℓ:

$$\{F(j)\} = [JFT]\{f(j)\} = [JFT][\mathfrak{x}_1 : \mathfrak{x}_2 : \mathfrak{x}_3]\begin{Bmatrix} \delta(i) \\ f(i) \\ \ell \end{Bmatrix}$$

$$\{\Delta(j)\} = [JDT]\{\delta(j)\} = [JDT][\mathfrak{y}_1 : \mathfrak{y}_2 : \mathfrak{y}_3]\begin{Bmatrix} \delta(i) \\ f(i) \\ \ell \end{Bmatrix} \tag{57}$$

where the [JFT] and [JDT] are coordinate transformation matrices from the local (dashed) system to the global (solid) system (see Fig. 8), and the $\mathfrak{x}_i$, $\mathfrak{y}_i$ matrices are obtained from the integration. Note that the effects of geometric nonlinearity are included in the $\mathfrak{x}_i$, $\mathfrak{y}_i$ terms. The loading, ℓ, consists of the applied distributed loads, thermal loads, and inelastic loads as defined by the inelastic stress resultants given in Eq. (7). The increments of plastic strain used to determine the quantities of Eq. (7) are taken to be those computed at the end of the current load step. These are used to predict the displacements at the end of the next load step. The equations above can be transformed into stiffness matrix form:

$$\{F(i)\} = [IFT][\mathfrak{y}_2]^{-1}([JDT]^T\{\Delta(j)\} - [\mathfrak{y}_1][IDT]^T\{\Delta(i)\} - [\mathfrak{y}_3]\{\ell\})$$

$$\{F(j)\} = [JFT][\mathfrak{x}_1][IDT]\{\Delta(i)\} + [JFT][\mathfrak{x}_2][\mathfrak{y}_2]^{-1}([JDT]^T\{\Delta(j)\}$$

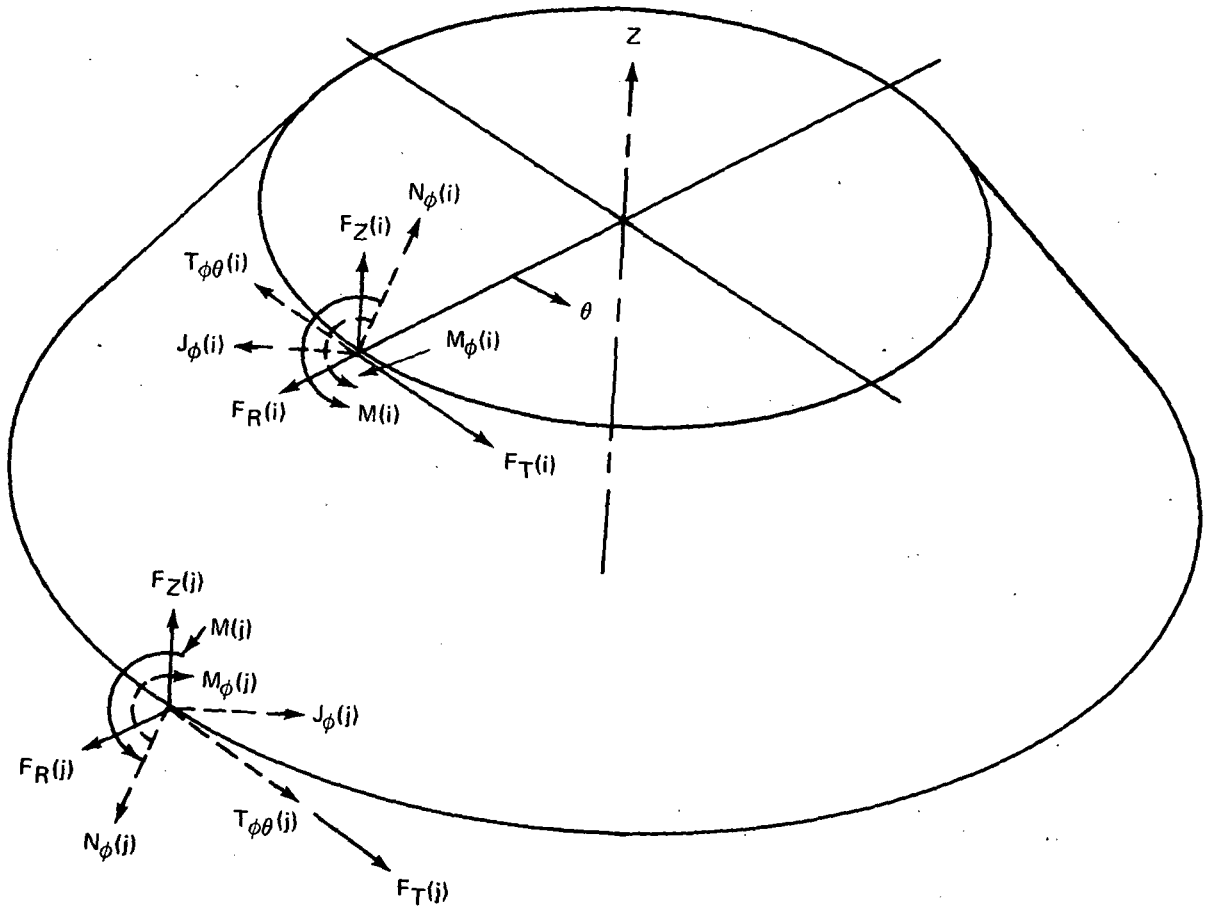

Fig. 8 Coordinate Systems

$$-[\mathcal{Y}_1][\mathrm{IDT}]^T\{\Delta(i)\} - [\mathcal{Y}_3]\{\ell\}) + [\mathrm{JFT}][\mathfrak{X}_3]\{\ell\} \tag{58}$$

(iii) Having thus defined the shell segment stiffness and load matrices from the integration procedure, the program needs to know whether there is enough basic region capacity (1 segment = 1 region) to idealize the structure, or whether multi-segment regions are to be used. If the former is true, proceed to step (iv).

If multi-segment regions are to be employed, a matrix reduction procedure (Guyan, Ref. [43]) must be used. The segments are first grouped by order, and then the overall region stiffness and load matrices are reduced to matrices relating only the region end points.

(iv) After completion of the region matrix manipulations, the direct stiffness matrix approach is used for the over-all problem solution. The results of such a solution procedure are the displacement vectors $\{\Delta\}$, for all the region joints in the shell. Utilizing the matrices obtained during Guyan reduction for each region, the displacement vector is expanded until it includes the displacements for all the segment ends throughout the shell structure.

(v) Utilizing the displacement solution for each segment in Eq. (58) we can obtain the forces $\{F\}$, at every joint. Since the segment grid is allowed to be rather coarse, and is chosen on the basis of geometric parameters rather than load or expected stress distributions, a final numerical integration on the complete Eq. (16) and (17) is performed at this stage to obtain a full stress and displacement increment distribution within all the shell segments. The initial vector for this final integration is the $\{F(i)\}$ and $\{\Delta(i)\}$ obtained from the over-all matrix solution. An automatic checking procedure is available at this stage in the solution since the $\{F(i)\}$, $\{\Delta(i)\}$ obtained from the over-all matrix solution and the $\{F(j)\}$, $\{\Delta(j)\}$ obtained from the final integration must satisfy the appropriate joint equilibrium and continuity equations.

Special Considerations Relating to Plasticity Analysis

Since the current program uses an incremental formulation, both total and incremental values of the necessary displacement and stress resultant variables in Eq. (16-17) must be kept. Thus as each load increment is completed the accumulated values are updated using Eq. (15), and thence utilized as the Y_{C_i} values in the next incremental pass through Eq. (16-17). Special calculations are also made due to the plasticity analysis as follows:

(i) At the end of each incremental step in the analysis, inelastic loads as defined by the inelastic stress resultants given in Eqs. (7) are calculated if the cross section is in the plastic range. The increments of plastic strain used to determine the necessary quantities of Eq. (7) are taken to be those computed at the end of the current load step.

Three basic shell wall cross sections are incorporated into the STARS-2P program. These are a solid cross section, and a sandwich cross section with equal, and unequal, thickness face sheets. Plastic effects are included by evaluating the plastic strains at prescribed points through the thickness, and thence obtaining the "inelastic forces and moments" [Eq. (7)] by integrating the plastic strain through the thickness using Simpson's rule. Up to 20 layers may be specified for the solid cross section. For sandwich sections, up to eight layers in each face sheet are allowed. The number of layers may be varied from segment to segment. These inelastic forces and moments are then incorporated into the next increment load vector, $\{\ell\}$, in Eq. (58), in the same manner as thermal forces and moments.

For smeared rings and stringers, the stresses and strains are evaluated only at the centroid of the stiffeners in the direction normal to their cross section. The centroidal offset distance is specified by the user. For rings, inelastic forces and moments with respect to the shell reference surface are obtained as:

$$N_{I\theta} = EA_R\epsilon_\theta^P \qquad M_{I\theta} = EA_R z_C \epsilon_\theta^P \tag{59}$$

These are summed with the plastic resultants obtained for the basic shell wall cross sections. To calculate the plastic strains in the rings, uniaxial stress-strain relations are employed. Smeared stringers are treated in a similar manner except that the meridional strain at the stringer centroid is calculated instead of the circumferential strain.

For the plastic analysis of waffle and isogrid reinforcements, the two dimensional state of strain in the shell is transformed into the directions of the reinforcements, whose centroids are offset a prescribed amount from the shell middle surface (the Kirchoff-Love assumption that normals remain straight and normal is assumed to hold). Uniaxial stress-strain relations are then used to calculate plastic strains and stresses in the stiffeners. "Inelastic forces" are then calculated in each reinforcement direction and are back-transformed into the shell coordinates and added to those found for the basic shell wall cross section. For all smeared reinforcement cases the inelastic forces and moments are incorporated into the segment load vectors, $\{\ell\}$, as noted previously.

A detailed stress analysis of isogrid, waffle, or other smeared sections is not obtained using the previous approximations. However, general load paths and the redistribution of forces may be obtained from the analysis. In addition, critical regions requiring a more refined inelastic analysis will be indicated. If one is interested in the local behavior in the vicinity of stringers or waffle or isogrid construction, then a nonaxisymmetric analysis must be employed.

In instances where detailed stress analysis is required, or the ring spacing is too large, the use of a "smeared" ring is inadequate. Discrete rings with nine possible cross sections are included in STARS-2P for such cases. These thin ring elements are based on curved beam theory, Ref. [44], com-

patible with the shell theory. The details of the linear elastic theory and its incorporation into STARS are presented in Ref. [26]. Transverse shear strains and cross sectional warping are neglected, however, the shear center and centroid need not coincide.

The plastic ring strains are calculated at discrete points on the ring cross section, and are integrated over the area using Gauss-Legendre integration to determine inelastic forces and moments, e.g.,

$$N_\theta^I = \int E\epsilon_\theta^P dA \qquad M_R^I = \int E\epsilon_\theta^P z dA \tag{60}$$

These are added to any thermal terms that are present, and incorporated as external loads acting on the ring. These loads are then used as part of the line load vector in the post Guyan reduction stiffness analysis.

(ii) It has been noted, Refs. [8 and 45], that the use of an incremental formulation may require equilibrium corrections for larger nonlinearities. This type of correction is automatically provided in STARS-2P at every integration point. The accumulated stress and deformation state in the shell is obtained from Eq. (15). This state is then substituted into the total form of the differential equations [Eq. (13a-f) and (13h-j)], where all the quantities can be thought of as having the subscript C_i. These equations are not identically satisfied because the inelastic strains used as effective forces to calculate the current displacements were assumed to be those computed at the end of the previous step. These predicted plastic strains are not exactly correct, leading to "remainders" to the identities [Eq. (13)]. These remainders are the R_i terms which may be found in Eq. (16). They are "pseudo load" additives to the segment load vectors as a correction term to be utilized in the next step. In this fashion, total equilibrium and strain compatibility is maintained in the shell structure throughout the loading history, and excessive drifting from the exact stress-strain curve is prevented.

CHAPTER 4

NUMERICAL EXAMPLES

To test the accuracy of the STARS-2P analysis several test problems were chosen and the results compared with available analytical and/or experimental data.

Circular Plate Under Monotonic Loading

First let us consider a circular plate under a monotonically increasing central load. This problem was originally considered in Ref. [9] where experimental results up to a total load of 500 pounds were presented. The geometry of the plate is shown in Fig. 9, along with a load versus central deflection curve. Also shown on the curve are the results from BOSOR5, Ref. [21], up to 1000 pounds. Experimental load-deflection data is presented here up to a 1000 pound total load and the additional data was obtained from Ref. [46]. The material properties used in the analysis correspond to a Ramberg-Osgood representation of the stress-strain data, Ref. [9], given by:

$$\epsilon = 10^{-6}(0.0953\sigma + 2.80\times10^{-12}\sigma^{3.661}) .$$

The specimen was made of 2024-0 aluminum alloy.

The results for STARS-2P compare extremely well with the experimental data up to the 1000 pound value. The predicted deflections are always slightly greater than the experimental data, with the worst discrepancies of about 10% occurring in the vicinity of $P = 250$ pounds. This corresponds to a large portion of the plate being in the knee of the stress-strain curve. A load increment of 5.5 pounds up to a maximum load of 1104 pounds was used. Another run using load steps of 11 pounds differed only slightly from the results presented, indicating a converged solution. The equilibrium correction term was used at every load step. Subsequent runs on a UNIVAC 1108 computer rather than an IBM 370, showed that the number of load steps could be halved again without significant accuracy changes on this machine.

Buckling of a Spherical Cap Under Uniform External Pressure

Next we consider a simply-supported isotropic spherical cap under a uniform external pressure. Wilkinson and Fulton considered the plastic buckling of such a cap in Ref. [47]. They assumed that the material obeyed a linear strain hardening law with a ratio of tangent modulus to Young's modulus of 0.1 and yield stress to Young's modulus of 0.002. A shell geometry parameter $\lambda = 2[3(1-\nu^2)]^{1/4}(H/h)^{1/2}$ equal to 4.0 was chosen, where ν is Poisson's ratio, H, the maximum shell rise, and h, the shell thickness. Other geometric quantities are defined in Fig. 10. The load-deflection curve for this shell is also given in Fig. 10. Initial yield occurs at a load of 900 psi, and buckling occurs at a load of 2150 psi which is 1.4% below the value of 2181 psi predicted by Wilkinson and Fulton.

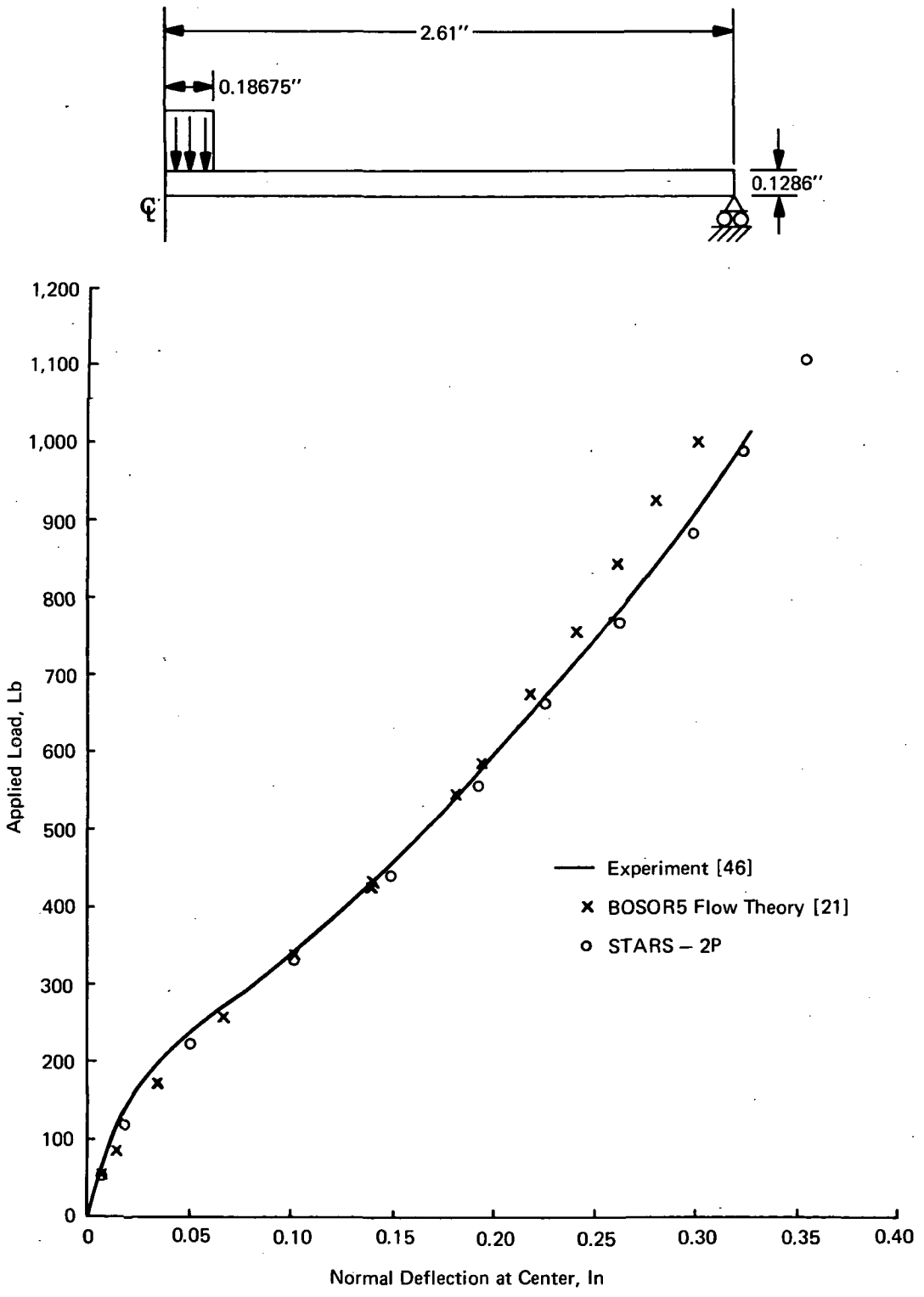

Fig. 9 Load-Deflection for Centrally Loaded Circular Plate

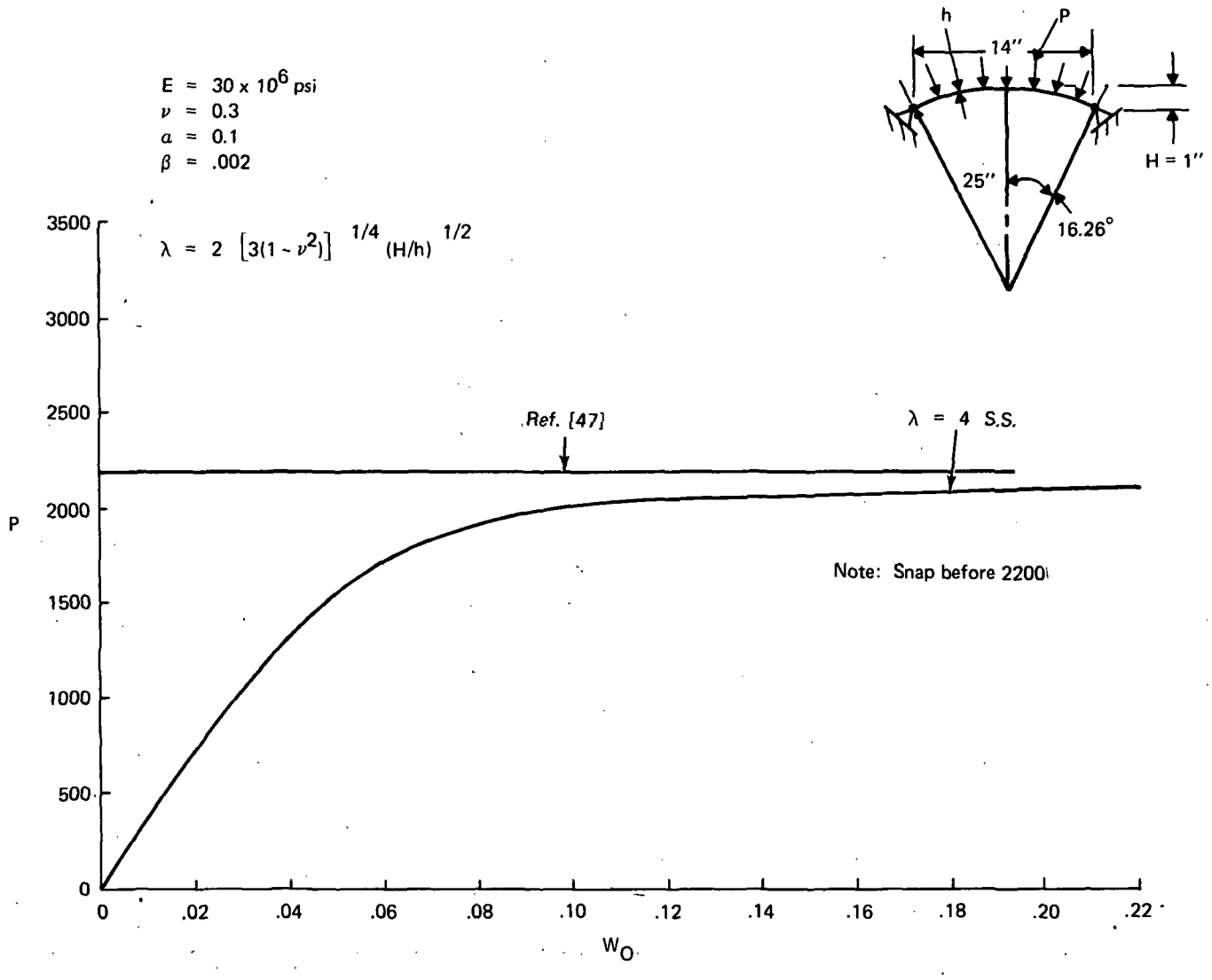

Fig. 10 Elasto-Plastic Buckling of Simply Supported Spherical Cap Under Uniform External Pressure, Load vs Central Deflection Curve

Plastic Buckling of a Sandwich Spherical Cap

Sharifi and Popov, Ref. [48], consider the buckling of a sandwich spherical cap under uniform external pressure. They use a finite element analysis which accounts for the elastic core stiffness and transverse shear deformation, but the core is assumed to remain elastic and only the face sheets are allowed to go plastic. They compare their results with the theoretical linear (eigenvalue) analysis of Yao, Ref. [49], and some experimental work performed by Lin, Ref. [50]. The latter comparison is inappropriate for the present purpose since it was observed that the cap buckled asymmetrically, and the results of Yao, Sharifi and Popov, and STARS-2P all assume an axisymmetric buckling mode.

The geometry of the cap and its material properties are shown in Fig. 11. Also indicated in the figure are the buckling load calculated by Yao ($P^* = 1$), the experimental buckling load (significantly lower than the axisymmetric mode), the load-deflection curve of Sharifi and Popov, and that calculated by STARS-2P. The deflection is that at a point located at $r/a = 0.69$, which is the point with the largest deflection for this structure. The STARS analysis apex deformation results are also shown. Sharifi predicts buckling at a load slightly below the linear (eigenvalue) analysis of Yao. The STARS-2P analysis predicts a buckling load of $P^* = 1.045$ which is approximately 5.5% higher than that of Sharifi and Popov. This might be due to the fact that the core in STARS-2P is assumed to be a rigid spacer between the face sheets. Despite this difference in the model, the analytical results compare reasonably well.

Plastic Buckling of an End-Loaded Clamped Circular Cylinder

We next consider a circular cylindrical shell clamped at both ends and subjected to a uniform edge compression. Pertinent dimensions are given in Fig. 12, and the material is 6061-0 aluminum alloy. Material properties were derived from data obtained from the Materials Selector Handbook and verified in the Grumman Research Department Applied Mechanics Laboratory. The Ramberg-Osgood parameters used were $E = 10^7$ psi, $\sigma_{0.7} = 5050$ psi, and $n = 4.8$. A proportional limit of 4300 psi was used. This cylinder was the subject of an experimental investigation performed at NASA/Langley Research Center. Figure 12 shows the experimental load-deflection curve up to initial buckling, Ref. [51], together with the one predicted by STARS-2P. The STARS program predicts a buckling load very close to that obtained experimentally, however, the predicted deflections are always larger than the experimental data.

The load-deflection data for this structure is very dependent upon the shape of the stress-strain curve. Additionally it was found that stress-strain data for 6061-0 alloy can vary considerably depending on material thickness and shape (i.e., sheet or rod). Since the material data used was not obtained from the specimen tested, it is possible that the experimental and theoretical stress-strain curves differed considerably.

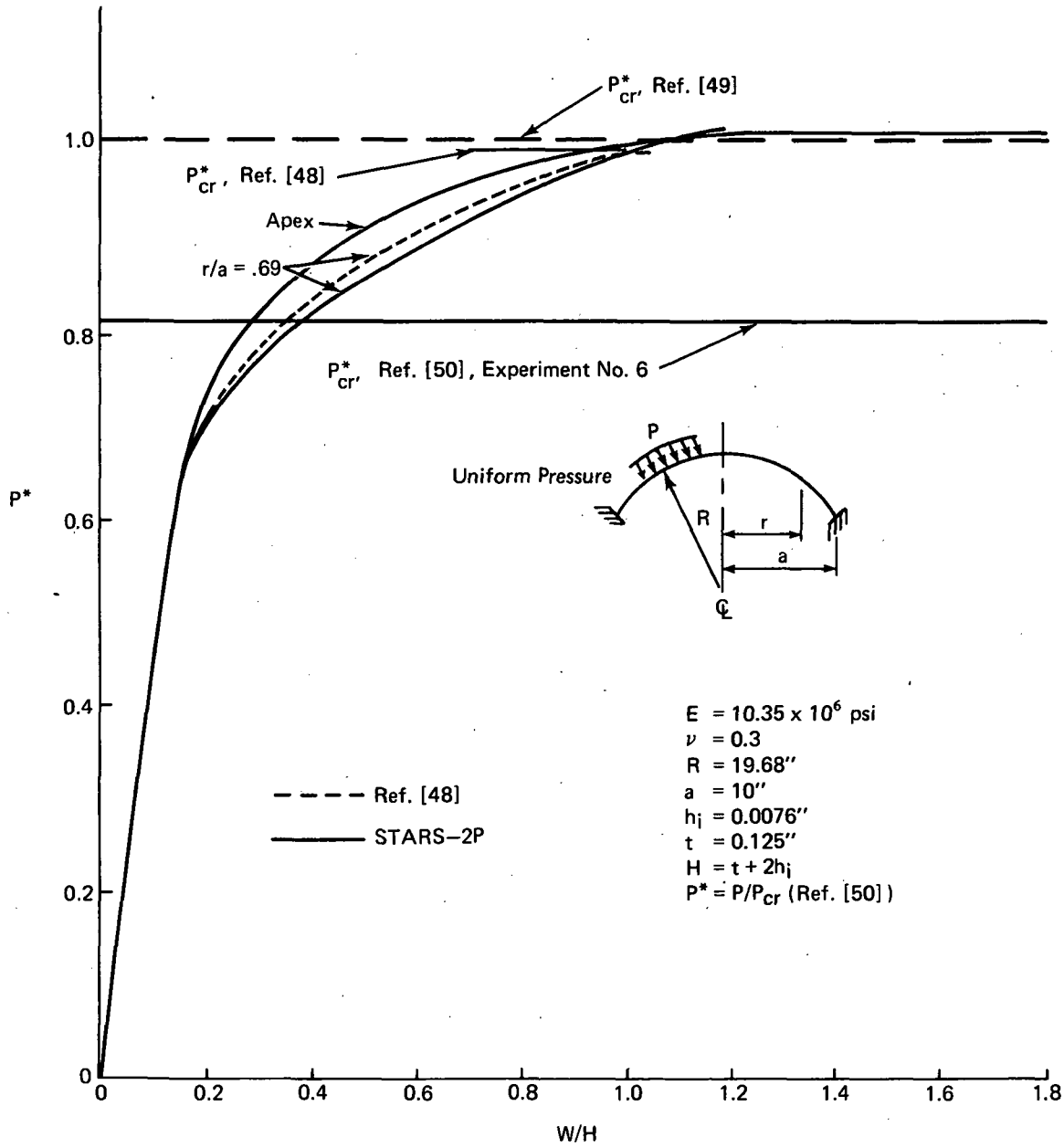

Fig. 11 Elastic-Plastic Buckling of Sandwich Cap

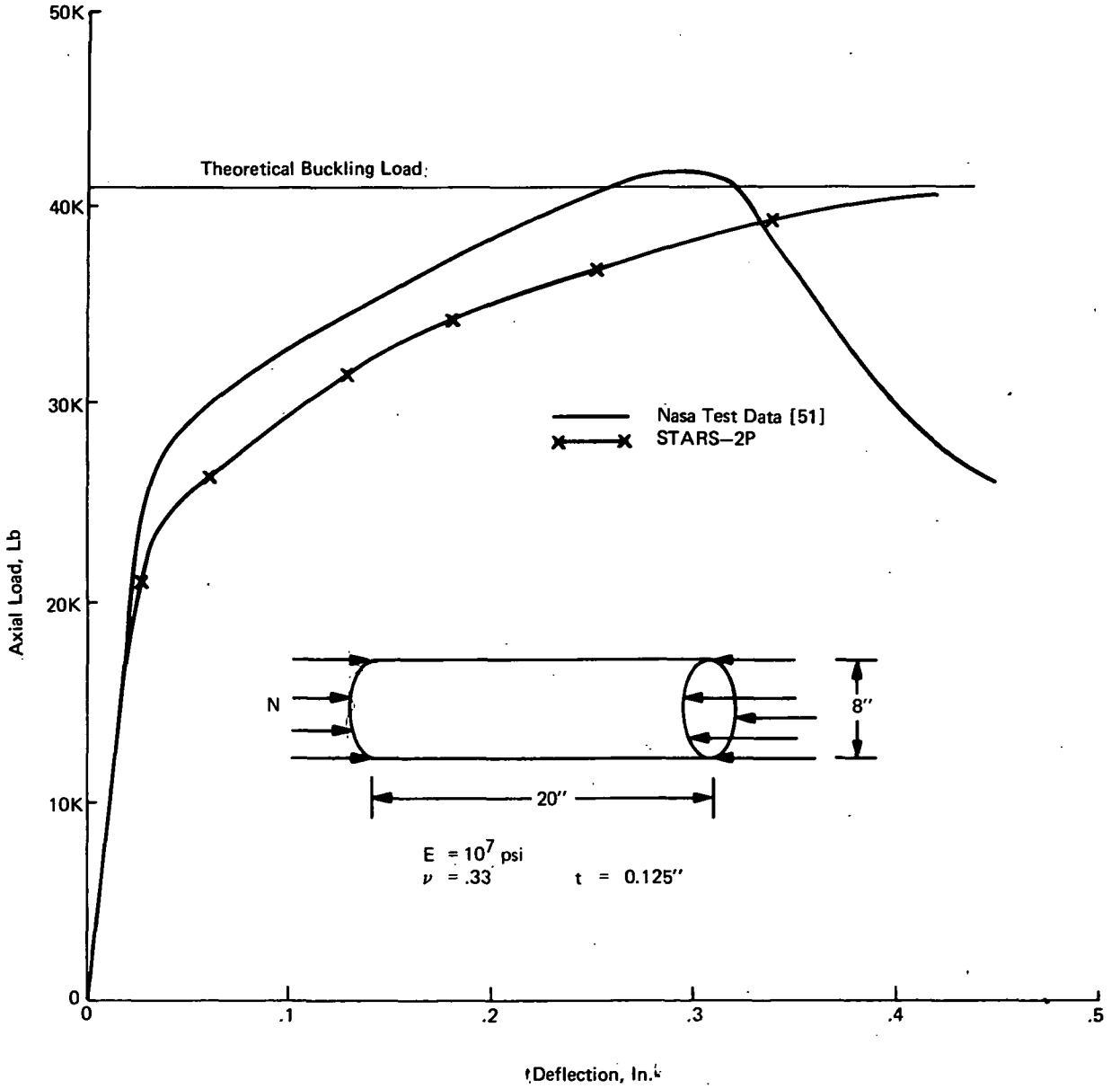

Fig. 12 Axial Load vs Cylinder End Deflection

Cyclic Behavior of a Centrally Loaded Circular Plate

The final test problem considered is that of a circular plate centrally loaded by a circular punch, and resting on a circular outer edge support. The geometry of the plate and a diagram of the load history is shown in Fig. 13. This plate was the subject of an experimental investigation performed at Grumman, Ref. [52]. The monotonic stress-strain curve for the 2024-0 aluminum alloy was presented in Ref. [9]. The Ramberg-Osgood representation of the monotonic stress-strain curve used in STARS-2P for this problem is:

$$\epsilon = 10^{-6}(0.0995\sigma + 9.634\times 10^{-14}\sigma^{3.967}) .$$

Since no cyclic stress-strain tests for this material were available, it was assumed that the monotonic and cyclic stress-strain curves coincided. To get the size and shape of the actual hysteretic stress-strain loops the representation proposed by Morrow, Ref. [41], was employed (see Chapter 2 for the calculation of the hardening coefficient). The comparison of the experimental and theoretical load versus plate central deflection curves is presented in Fig. 14 for the loading pattern shown in Fig. 13. Kinematic hardening theory was used in the analysis.

Considering that the cyclic stress-strain curve is unknown, the correlation is quite acceptable. There is an initial over-prediction of the deflection at the maximum load (P = 1320 pounds). The elastic unloading curves are parallel and the shape and size of the hysteretic curves are quite similar if one allows for the initial overprediction. Near the minimum load (P = – 770 pounds) the theoretical strains increase more rapidly than do the experimental strains. This may demonstrate that the actual material does not exhibit an ideal Bauschinger effect, and thus the predicted theoretical plastic strains are larger than the actual ones. Upon reloading to P = 1320 pounds, the theoretical results predict slightly larger deflections than those produced after the initial loading while the experiment shows slightly smaller deflections. The initial overprediction and consequent cycling between different strain ranges may account for this difference. Examination of the stresses and strains at the top and bottom surfaces revealed that for this $\frac{1}{4}$-inch thick plate geometric nonlinearity was negligible.

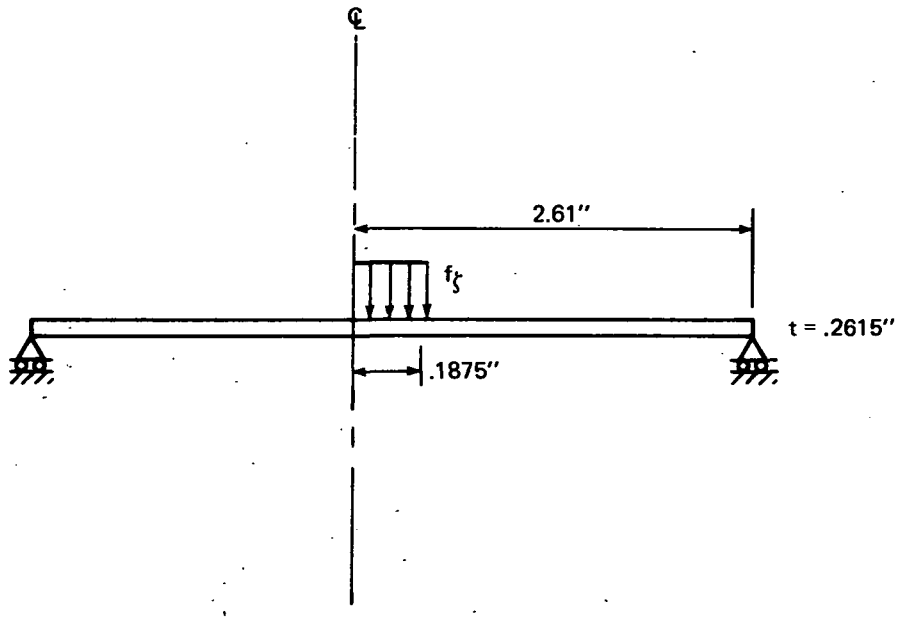

(a) Structure

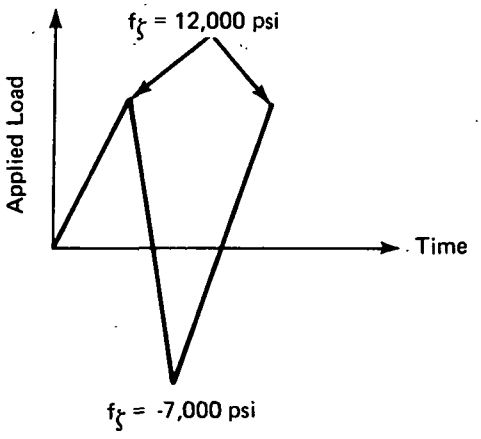

(b) Loading Pattern

Fig. 13 Circular Plate Under Cyclic Loading

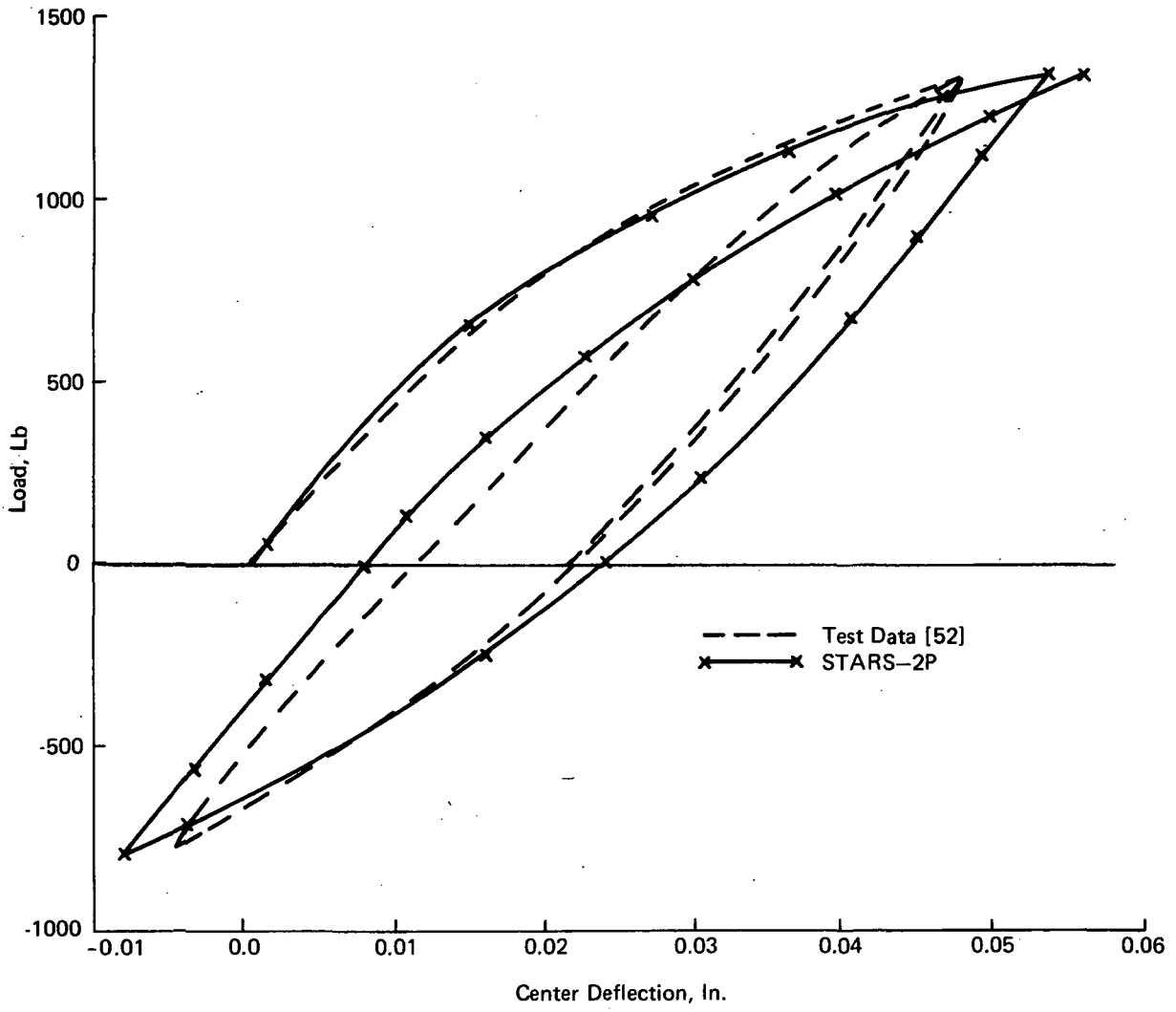

Fig. 14 Cyclic Load - Deflection Curve at Center of Circular Plate

REFERENCES

1. Marcal, P. V., "Large Deflection Analysis of Elastic-Plastic Shells of Revolution," Proceedings of the 10th ASME/AIAA Structures, Structural Dynamics, and Materials Conference, April 1969.
2. "MARC-CDC Nonlinear Finite Element Analysis Program," User Information Manual, Vol. 1, Control Data Corp., 1971.
3. Khojasteh-Bakht, M., "Analysis of Elastic-Plastic Shells of Revolution under Axisymmetric Loading by the Finite Element Method," Ph.D. Dissertation, Dept. of Civil Engrg., Univ. of Calif., Berkeley, 1967.
4. Yaghmai, S., "Incremental Analysis of Large Deformations in Mechanics of Solids with Applications to Axisymmetric Shells of Revolution," NASA CR-1350, June 1969.
5. Zudans, Z., "Finite Element Incremental Elastic-Plastic Analysis of Pressure Vessels," Trans. ASME, Journal of Eng. for Industry, Vol. 92, 1970.
6. Zudans, Z., et al., "Theory and User's Manual for EPACA," Franklin Institute Report F-C-3038, June 1972.
7. Zudans, Z., Reddi, M., Tsai, H., and Huber, A., "DYPLAS – A Finite Element Dynamic Elastic-Plastic Large Deformation Analysis Program," 2nd International Conference on Structural Mechanics in Reactor Technology, W. Berlin, September 1973.
8. Stricklin, J., Haisler, W., and Von Riesemann, W., "Formulation, Computation, and Solution Procedures for Material and/or Geometric Nonlinear Structural Analysis by the Finite Element Method," Texas A & M University and Sandia Corporation Report SC-CR-72-3102, January 1972.
9. Levine, H. S., Armen, H. Jr., Winter, R., and Pifko, A., "Nonlinear Behavior of Shells of Revolution under Cyclic Loading," Computers and Structures, Vol. 3, pp. 589-617, 1973.
10. Stricklin, J., et al., "Large Deflection Elastic-Plastic Dynamic Response of Stiffened Shells of Revolution," Texas A & M University, TEES-RPT-72-25, December 1972.
11. Novozhilov, V., The Theory of Thin Shells, P. Noordhoff, Groningen, Netherlands, 1964.
12. Armen, H. Jr., "Plastic Analysis," Proceedings of International Symposium on Structural Mechanics Software, Univ. of Md., June 1974.
13. Pifko, A., Levine, H., and Armen, H. Jr., "PLANS – A Finite Element Program for Nonlinear Analysis of Structures," Grumman Research Department Report (to be published).
14. De Salvo, G., and Swanson, J., "ANSYS Engineering Analysis Systems Manual," Swanson Analysis Systems, Inc., October 1972.
15. Sharifi, P., and Yates, D., "Nonlinear Thermo-Elastic-Plastic and Creep Analysis by the Finite Element Method," AIAA Paper No. 73-358, 14th Structures Conference, March 1973.
16. Balmer, H., "Improved Computer Programs: DEPROSS 1, 2, and 3, to Calculate the Dynamic Elastic-Plastic Two Dimensional Responses of Impulsively Loaded Beams, Rings, Plates, and

Shells of Revolution," MIT, ASRL TR 128-3, August 1965.

17. McCallum, R., "CRASH 12: A Computer Program to Calculate Dynamic Elastic-Plastic Response of a Free Nonuniformly Heated Ring Subjected to Arbitrary Sequential Loadings," MIT, ASRL TR 135-3, September 1967.
18. Krieg, R., and Duffey, T., "UNIVALVE II: A Code to Calculate the Large Deflection Dynamic Response of Beams, Plates, and Cylinders," Sandia Lab. Report SC-RR-303, October 1968.
19. Morino, L., Leech, J., and Witmer, E., "An Improved Numerical Calculation Technique for Large Elastic-Plastic Transient Deformations of Thin Shells, Part 1 – Background and Theoretical Formation," ASME Journal of Applied Mechanics, pp. 423-428, June 1971.
20. Morino, L., Leech, J., and Witmer, E., "An Improved Numerical Calculation Technique for Large Elastic-Plastic Transient Deformations of Thin Shells, Part 2 – Evaluation and Applications," ASME Journal of Applied Mechanics, pp. 429-436, June 1971.
21. Bushnell, D., "Large Deflection Elastic-Plastic Creep Analysis of Axisymmetric Shells," Numerical Solution of Nonlinear Structural Problems, Proceedings of the ASME Winter Meeting, November 1973.
22. Engeli, M., Ginsburg, T., Rutishauser, H., and Stiefel, E., "Redefined Iterative Methods for Computation of the Solution and the Eigenvalues of Self-Adjoint Boundary Value Problems," Mitt. Inst. Ang. Math., No. 8, Zurich, 1959.
23. Havner, K., "On Convergence of Iterative Methods in Plastic Strain Analysis," Int. Journal of Solids and Structures, Vol. 4, pp. 491-508, 1968.
24. Gerdeen, J. C., Simonen, F. A., and Hunter, D. T., "Large Deflection Analysis of Elastic-Plastic Shells of Revolution," AIAA J., Vol. 9, No. 6, June 1971.
25. Sanders, J. L. Jr., "An Improved First Approximation Theory for Thin Shells," NASA Report 24, June, 1959.
26. Svalbonas, V., "Numerical Analysis of Stiffened Shells of Revolution – Vol. I," NASA CR-2273, September 1973.
27. Kempner, J., "Unified Thin Shell Theory," Polytechnic Institute of Brooklyn, PIBAL Report No. 566, March 1960.
28. Hill, R., The Mathematical Theory of Plasticity, Chapter 12, Oxford Univ. Press, 1950.
29. Ramberg, W., and Osgood, W. R., "Description of Stress-Strain Curves by Three Parameters," *NACA TN-902, 1943.*
30. Mendelson, A., and Manson, S., "Practical Solution of Plastic Deformation Problems in the Elastic-Plastic Range," NASA TR-R-28, 1959.
31. Hildebrand, F. B., Introduction to Numerical Analysis, McGraw-Hill, New York, 1965.

32. Drucker, D. C., "A More Fundamental Approach to Plastic Stress-Strain Relations," Proceedings of the 1st U. S. National Congress of Applied Mechanics, p. 487, 1952.

33. Prager, W., "A New Method of Analyzing Stress and Strains in Work Hardening Plastic Solids," J. Applied Mechanics, Vol. 23, p. 493, 1956.

34. Ziegler, H., "A Modification of Prager's Hardening Rule," Quart. of Appl. Math., Vol. 17, No. 1, p. 55, 1959.

35. Mendelson, A., Plasticity: Theory and Application, MacMillan and Co., New York, 1968.

36. Armen, H. Jr., Pifko, A., and Levine, H. S., "Finite Element Analysis of Structures in the Plastic Range," NASA CR-1649, February 1971.

37. Hunsaker, B. Jr., Vaughan, D., Stricklin, J., and Haisler, W., "A Comparison of Current Work Hardening Models Used in the Analysis of Plastic Deformations," Texas A & M Report TEES-RPT-2926-73-3, October 1973.

38. Levine, H. S., "A Hardening Coefficient for Orthotropic Kinematic Hardening," Grumman Research Department Report (in preparation).

39. Tsai, S., and Wu, E., "A General Theory of Strength for Anisotropic Materials," J. Composite Materials, Vol. 5, p. 58, January 1971.

40. RDT Standard, RDT F9-4, Requirements for Design of Nuclear System Components at Elevated Temperatures (Supplement to ASME Code Case 1331) – Vol. II, December 1973.

41. Morrow, J., "Cyclic Plastic Strain Energy and Fatigue of Metals," ASTM STP No. 378, 1965.

42. Yamada, T., Kawai, T., Yoshimura, N., and Sakurai, T., "Analysis of the Elastic Plastic Problems by the Matrix Displacement Method," AFFDL-TR-68-150, February 1970.

43. Guyan, R., "Reduction of Stiffness and Mass Matrices," AIAA Journal, Vol. 3, No. 2, February 1965.

44. Cheney, J., "Bending and Buckling of Thin-Walled Open Section Rings," ASCE Proceedings, EM-5, pp. 17-44, October 1963.

45. Hofmeister, L., Greenbaum, G., and Evensen, D., "Large Strain Elasto-Plastic Finite Element Analysis," AIAA J., Vol. 9, No. 7, p. 1248, 1971.

46. Winter, R., "Experiments on Large Plastic Deformations of Circular Plates with Work Hardening," Grumman Research Department Report (in preparation).

47. Wilkinson, M., and Fulton, R., "Axisymmetric Buckling of Uniformly Loaded Spherical Caps Undergoing Plastic Deformation," to be published in AIAA J.

48. Sharifi, P., and Popov, E. P., "Nonlinear Finite Element Analysis of Sandwich Shells of Revolution," Proceedings of the 13th Structures, Structural Dynamics, and Materials Conference, April 1972.

49. Yao, J. C., "Buckling of a Sandwich Sphere Under Normal Pressure," J. Aero. Sci., pp. 264-268, March 1962.

50. Lin, M. S., "Buckling of Spherical Sandwich Shells," Ph.D. Dissertation, University of California, December 1968.

51. Thomson, R., NASA Langley Research Center, Private Communication, 1972.

52. Winter, R., "Experiment on Cyclic Plastic Deformations of a Circular Plate with Work Hardening," Grumman Research Department Report (in preparation).

APPENDIX

CONVERSION OF U. S. CUSTOMARY UNITS TO SI UNITS

The International System of Units (SI) was adopted by the Eleventh General Conference on Weights and Measures in 1960. Conversion factors for the units used in this report are given in the following table:

Physical quantity	U. S. Customary Unit	Conversion factor (*)	SI Unit (**)
Length	in.	0.0254	meters
Stress modulus	ksi	6.895×10^6	newtons/meter^2 (N/m^2)
Stress resultant	lbf/in.	175.1	newtons/meter (N/m)
Temperature change	°F	5/9	Kelvin (K)

*Multiply value given in U. S. Customary Units by conversion factor to obtain equivalent value in SI Units.

**Prefixes to indicate multiple of units are as follows:

Prefix	Multiple
giga (G)	10^9
mega (M)	10^6
kilo (k)	10^3
deci (d)	10^{-1}
centi (c)	10^{-2}
milli (m)	10^{-3}

NASA-Langley, 1975

NATIONAL AERONAUTICS AND SPACE ADMINISTRATION
WASHINGTON, D.C. 20546

OFFICIAL BUSINESS
PENALTY FOR PRIVATE USE $300

SPECIAL FOURTH-CLASS RATE BOOK

POSTAGE AND FEES PAID
NATIONAL AERONAUTICS AND SPACE ADMINISTRATION
451

POSTMASTER: If Undeliverable (Section 158 Postal Manual) Do Not Return

"The aeronautical and space activities of the United States shall be conducted so as to contribute . . . to the expansion of human knowledge of phenomena in the atmosphere and space. The Administration shall provide for the widest practicable and appropriate dissemination of information concerning its activities and the results thereof."

—NATIONAL AERONAUTICS AND SPACE ACT OF 1958

NASA SCIENTIFIC AND TECHNICAL PUBLICATIONS

TECHNICAL REPORTS: Scientific and technical information considered important, complete, and a lasting contribution to existing knowledge.

TECHNICAL NOTES: Information less broad in scope but nevertheless of importance as a contribution to existing knowledge.

TECHNICAL MEMORANDUMS: Information receiving limited distribution because of preliminary data, security classification, or other reasons. Also includes conference proceedings with either limited or unlimited distribution.

CONTRACTOR REPORTS: Scientific and technical information generated under a NASA contract or grant and considered an important contribution to existing knowledge.

TECHNICAL TRANSLATIONS: Information published in a foreign language considered to merit NASA distribution in English.

SPECIAL PUBLICATIONS: Information derived from or of value to NASA activities. Publications include final reports of major projects, monographs, data compilations, handbooks, sourcebooks, and special bibliographies.

TECHNOLOGY UTILIZATION PUBLICATIONS: Information on technology used by NASA that may be of particular interest in commercial and other non-aerospace applications. Publications include Tech Briefs, Technology Utilization Reports and Technology Surveys.

Details on the availability of these publications may be obtained from:

SCIENTIFIC AND TECHNICAL INFORMATION OFFICE

NATIONAL AERONAUTICS AND SPACE ADMINISTRATION

Washington, D.C. 20546